

STABILITY AND CONVERGENCE OF MIXED FINITE ELEMENTS FOR LINEAR REGULARIZED 13-MOMENT EQUATIONS *

SHUANG HU[†], HUITENG LI[‡], AND ZHENNING CAI[§]

Abstract. We present a stable and convergent mixed finite element method (MFEM) for the linear regularized 13-moment (R13) equations in rarefied gas dynamics. Unlike existing methods that require stabilization via penalty terms, our scheme achieves inherent stability by enriching the finite element basis with bubble functions. We provide a rigorous theoretical analysis, establishing second-order convergence rates in the L^2 norm under mild regularity assumptions. Beyond theoretical properties, our scheme demonstrates practical advantages over standard MFEM schemes, yielding robust numerical results even in the presence of geometric singularities.

Key words. Regularized 13-moment equations, rarefied gas dynamics, mixed finite element method, discrete inf-sup condition, Korn-type inequalities.

MSC codes. 65N30, 65N12, 76P05.

1. Introduction. In gas kinetic theory, moment methods have been playing important roles in the modeling and simulation of non-equilibrium flows. Since the moment method was first introduced by Grad [15] in 1949, numerous moment models have been proposed to improve the accuracy and stability of equations [17, 22, 20, 34], among which the regularized 13-moment (R13) equations, introduced in [32, 33], have been attracting much attention in the past two decades due to their good performance in various benchmark tests [37, 23, 40, 13]. While the original R13 equations were devised for Maxwell molecules, they have been generalized to other intermolecular potentials [9], and in all cases, the resulting equations enjoy both linear stability and super-Burnett order of accuracy. Recently, stable boundary conditions have been formulated for these equations, further enhancing their potential application in practical boundary value problems [27, 38]. Numerical experiments indicate that R13 equations allow simulations of rarefied gas dynamics with Knudsen number $\text{Kn} \sim 0.1$ without directly solving the Boltzmann equation [25].

While many moment models are gradually losing their attractiveness due to either robustness or accuracy issues, R13 equations stand as one of the models that are still being widely studied both theoretically and numerically. One obstacle to promoting the applications of R13 equations is the large number of variables in the system, more than twice as many as Euler/Navier-Stokes-Fourier equations. To address this issue, an easy-to-implement numerical method may be helpful. Recently, researchers have been studying linearized R13 equations, which are accurate in the slow-flow regime, and have established several breakthroughs. For instance, the method of fundamental solutions has been introduced in [12] and further developed in [16]. Also, significant progress has been made on the finite element method (FEM), a field to which our work will also contribute.

* Shuang Hu and Huiteng Li are co-first authors with equal contributions.

Funding: The work of Zhenning Cai was supported by the Academic Research Fund of the Ministry of Education of Singapore under Grant No. A-8002392-00-00.

[†] Zhejiang University, 866 Yuhangtang Road, Hangzhou, Zhejiang Province, 310058 China (hs-mathnna@gmail.com).

[‡] King Abdullah University of Science and Technology (KAUST), Thuwal, 23955 Saudi Arabia (huiteng.li@kaust.edu.sa).

[§] Corresponding author. Department of Mathematics, National University of Singapore, Level 4, Block S17, 10 Lower Kent Ridge Road, Singapore 119076 (matcz@nus.edu.sg).

Lately, the well-posedness of the steady-state linearized R13 equations for Maxwell molecules has been rigorously justified, marking another milestone in the theoretical study of moment equations [18] and providing a solid basis for the study of the finite element method. The weak form of R13 equations appears as a saddle-point problem, resembling the classical Stokes equations, for which the well-posedness can be established using Brezzi's theorem [6]. With such a structure, a natural choice of its numerical solver is the mixed FEM. However, since the 2010s, the development of FEM for R13 equations has undergone a bumpy road, accompanied by the formulation of its boundary conditions. Early attempts were documented in some master theses [21, 42], where the 13-moment equations were separated into a stress system and a heat flux system, which were solved independently for the purpose of a closer look at possible issues. Notably, when the subsystems were solved using the standard Taylor-Hood elements, oscillations were observed in velocity and temperature profiles near the curved boundary, causing significant L^∞ errors in the numerical solutions. The work [42] managed to suppress the oscillation using isoparametric elements with higher-order polynomials, and later in [43], the continuous interior penalty (CIP) method was adopted to obtain smooth numerical solutions for Taylor-Hood elements. Both works [42, 43] solved only a subsystem of the R13 equations and did not report any results on the full system.

Note that the boundary conditions used in these works were based on the formulation introduced in [41], which did not provide a symmetric weak form. In [24], thermodynamically admissible boundary conditions were formulated for R13 equations, which completely changed the landscape of FEM for R13 equations. Using the new boundary conditions, the variational form of the R13 equations was first presented with all boundary conditions inserted in a symmetric way [44], and FEM solutions without spurious oscillations on the curved boundary were finally obtained.

CIP stabilization, applied in all the successful FEM implementations mentioned above, requires a few extra parameters to be tuned, which may be problem-dependent. Can we have a solver without extra parameters? In [38], with a further adjustment of the boundary conditions, desired convergence rates were eventually achieved using \mathbb{P}_2 - \mathbb{P}_1 mixed elements without CIP stabilization. However, as we will show in section 5, this approach may still lead to instability in some cases. The work [38] introduces a software package known as `fenicsR13` [39], which provides a large number of test cases in both 2D and 3D cases.

It has been a long journey since the first attempts of FEM for R13 equations, a seemingly simple problem that turns out to be quite challenging. But the question of a robust and parameter-free FEM solver for R13 equations is still open. In this work, we would like to tackle this problem and continue the quest. Here we summarize our contributions as follows:

- We construct a stable, conforming mixed finite element method for the R13 system. Unlike existing approaches, our scheme does not require any artificial stabilization or penalty parameters.
- We establish the well-posedness of the discrete problem by proving the discrete inf-sup condition and deriving the a priori error estimates.
- We verify the validity of our scheme through various benchmarks. In particular, the scheme exhibits superior stability in problems lacking regularity, where standard schemes (e.g., Taylor-Hood) tend to fail.

While our solution is not the most computationally economical choice due to the enriched space, the overhead is relatively minor in 2D. More importantly, this cost is compensated for by the method's theoretical reliability. In contrast to CIP stabiliza-

tion, which lacks a rigorous convergence proof, we establish the well-posedness of our discrete problem and demonstrate that the scheme achieves second-order convergence in the L^2 norm.

The rest of the paper is organized as follows. Section 2 introduces the necessary notation and the weak formulation of the R13 system. In Section 3, we construct the mixed finite element scheme and define the associated finite element spaces. Section 4 is devoted to the theoretical analysis, establishing the discrete stability and convergence of the proposed method. Numerical experiments validating these results are reported in Section 5. Finally, Section 6 summarizes the work and discusses future research directions.

2. Preliminaries.

2.1. Notation. Let $\Omega \subseteq \mathbb{R}^d$ ($d = 2, 3$) be a bounded polygonal/polyhedral domain with boundary Γ . For any subdomain $D \subseteq \Omega$ and integer $m \geq 0$, let $H^m(D)$ denote the set of all $L^2(D)$ functions whose weak derivatives up to order m are also square-integrable. The spaces for vector-valued or tensor-valued functions are given by $H^m(D; \mathbb{X}) := H^m(D) \otimes \mathbb{X}$, with the norm $\|\cdot\|_{m,D}$ and semi-norm $|\cdot|_{m,D}$. The case $m = 0$ corresponds to the space of square-integrable functions, and we use $(\cdot, \cdot)_D$ to denote the standard L^2 -inner product on the domain D on $L^2(D)$ or $L^2(D; \mathbb{X})$. Denote by $H_0^m(D; \mathbb{X})$ the closure of $C_0^\infty(D; \mathbb{X})$ with respect to the norm $\|\cdot\|_{m,D}$. Denote by $H^{-1}(D; \mathbb{X})$ the dual of $H_0^1(D; \mathbb{X})$ with the induced norm $\|\cdot\|_{-1,D}$. When $D = \Omega$, the subscripts for norms, semi-norms and L^2 -inner products are abbreviated as $\|\cdot\|_m$, $|\cdot|_m$ and (\cdot, \cdot) , respectively. We denote by L_0^2 and \tilde{H}^1 the subspaces of L^2 and H^1 containing functions with zero mean, respectively. Throughout this paper, $A \lesssim B$ (resp., $A \gtrsim B$) denotes $A \leq CB$ (resp., $A \geq CB$) for a generic constant $C > 0$ independent of the mesh size. We write $A \simeq B$ if $A \lesssim B \lesssim A$.

For the R13 system, the tensor space \mathbb{T} is defined according to the dimension d :

$$(2.1) \quad \mathbb{T} := \begin{cases} \mathbb{R}_{\text{sym}}^{2 \times 2}, & d = 2, \\ \mathbb{R}_{\text{stf}}^{3 \times 3}, & d = 3, \end{cases}$$

where $\mathbb{R}_{\text{sym}}^{d \times d}$ and $\mathbb{R}_{\text{stf}}^{d \times d}$ denote the spaces of symmetric and symmetric trace-free matrices, respectively. We define the associated projection operators $\text{sym} : \mathbb{R}^{d \times d} \rightarrow \mathbb{R}_{\text{sym}}^{d \times d}$ and $\text{stf} : \mathbb{R}^{d \times d} \rightarrow \mathbb{R}_{\text{stf}}^{d \times d}$ as:

$$(2.2) \quad \text{sym } \boldsymbol{\sigma} := \frac{1}{2}(\boldsymbol{\sigma} + \boldsymbol{\sigma}^T), \quad \text{stf } \boldsymbol{\sigma} := \text{sym } \boldsymbol{\sigma} - \frac{1}{d}(\text{tr } \boldsymbol{\sigma}) \mathbf{I}_d.$$

The definition of the symmetric trace-free projection extends to third-order tensors ($d = 3$) through the operator $\text{Stf} : \mathbb{R}^{3 \times 3 \times 3} \rightarrow \mathbb{R}_{\text{stf}}^{3 \times 3 \times 3}$. For any $\mathbf{m} \in \mathbb{R}^{3 \times 3 \times 3}$, the components of $\text{Stf } \mathbf{m}$ are given by:

$$(2.3) \quad (\text{Stf } \mathbf{m})_{ijk} := m_{(ijk)} - \frac{1}{5} \sum_{l=1}^3 (m_{(ill)} \delta_{jk} + m_{(ljl)} \delta_{ik} + m_{(llk)} \delta_{ij}),$$

where the permutation sum $m_{(ijk)}$ is defined by $m_{(ijk)} := \frac{1}{6}(m_{ijk} + m_{jki} + m_{kij} + m_{jik} + m_{ikj} + m_{kji})$ and δ_{ij} is the Kronecker delta.

Finally, for brevity we define the dimension-dependent differential operator \mathcal{E} as

$$(2.4) \quad \mathcal{E} := \begin{cases} \text{sym } \nabla, & d = 2, \\ \text{stf } \nabla, & d = 3. \end{cases}$$

2.2. Regularized 13-moment system. The *regularized 13-moment* (R13) system governs the evolution of the following fields: the pressure $p : \Omega \rightarrow \mathbb{R}$, the velocity $\mathbf{u} : \Omega \rightarrow \mathbb{R}^3$, the temperature $\theta : \Omega \rightarrow \mathbb{R}$, the heat flux $\mathbf{s} : \Omega \rightarrow \mathbb{R}^3$, and the symmetric trace-free stress tensor $\boldsymbol{\sigma} : \Omega \rightarrow \mathbb{R}_{\text{stf}}^{3 \times 3}$. Since $\boldsymbol{\sigma}$ is symmetric and trace-free, it possesses 5 degrees of freedom, resulting in a total of 13 unknowns for the system.

The R13 system consists of the *conservation laws* for mass, momentum, and energy, and the *evolution equations* for the higher-order moments. The conservation laws are given by:

$$(2.5) \quad \begin{cases} -\nabla \cdot \mathbf{u} = 0, \\ \nabla p + \nabla \cdot \boldsymbol{\sigma} = 0, & \text{in } \Omega, \\ \nabla \cdot \mathbf{u} + \nabla \cdot \mathbf{s} = 0, \end{cases}$$

and the evolution equations describing the stress and heat flux are:

$$(2.6) \quad \begin{cases} \frac{4}{5} \text{stf } \nabla \mathbf{s} + 2 \text{stf } \nabla \mathbf{u} - 2 \text{Kn} \nabla \cdot (\text{stf } \nabla \boldsymbol{\sigma}) = -\frac{1}{\text{Kn}} \boldsymbol{\sigma}, \\ \frac{5}{2} \nabla \theta + \nabla \cdot \boldsymbol{\sigma} - \frac{12}{5} \text{Kn} \nabla \cdot (\text{stf } \nabla \mathbf{s}) - 2 \text{Kn} \nabla \cdot \mathbf{s} = -\frac{1}{\text{Kn}} \frac{2}{3} \mathbf{s}, \end{cases} \quad \text{in } \Omega.$$

Here, $\text{Kn} > 0$ denotes the Knudsen number.

Let $(\mathbf{t}_1, \mathbf{t}_2, \mathbf{n})$ be a boundary-aligned orthonormal frame with outer unit normal \mathbf{n} . For any $\mathbf{a}, \mathbf{b}, \mathbf{c} \in \{\mathbf{t}_1, \mathbf{t}_2, \mathbf{n}\}$, we define the projected components as $u_a := \mathbf{u} \cdot \mathbf{a}$, $\sigma_{ab} := \sum_{i,j} \sigma_{ij} a_i b_j$, and $m_{abc} := \sum_{i,j,k} m_{ijk} a_i b_j c_k$. By enforcing impermeability ($u_n = 0$) consistent with Maxwell's solid-wall model, the *Onsager boundary conditions* are formulated via higher-order moments \mathbf{m} , \mathbf{R} and Δ :

$$(2.7) \quad \begin{cases} u_n = 0, \\ \sigma_{nt_i} = \tilde{\chi} ((u_{t_i} - u_{t_i}^W) + \frac{1}{5} s_{t_i} + m_{nnt_i}) \quad (i \in \{1, 2\}), \\ R_{nt_i} = \tilde{\chi} (- (u_{t_i} - u_{t_i}^W) + \frac{11}{5} s_{t_i} - m_{nnt_i}) \quad (i \in \{1, 2\}), \\ s_n = \tilde{\chi} (2 (\theta - \theta^W) + \frac{1}{2} \sigma_{nn} + \frac{2}{5} R_{nn} + \frac{2}{15} \Delta), \\ m_{nnn} = \tilde{\chi} (-\frac{2}{5} (\theta - \theta^W) + \frac{7}{5} \sigma_{nn} - \frac{2}{25} R_{nn} - \frac{2}{75} \Delta), \\ (\frac{1}{2} m_{nnn} + m_{nt_1 t_1}) = \tilde{\chi} (\frac{1}{2} \sigma_{nn} + \sigma_{t_1 t_1}), \\ m_{nt_1 t_2} = \tilde{\chi} \sigma_{nt_1 t_2}. \end{cases} \quad \text{on } \Gamma,$$

Here, $\mathbf{u}_{t_i}^W$ and θ^W denote the wall tangential velocity and wall temperature, respectively, and $\tilde{\chi} > 0$ represents the modified Maxwell accommodation factor as introduced in [44]. The closures for higher-order moments \mathbf{m} , \mathbf{R} and Δ in (2.7) are given by

$$(2.8) \quad \mathbf{m} := -2 \text{Kn} \text{Stf } \nabla \boldsymbol{\sigma}, \quad \mathbf{R} := -\frac{24}{5} \text{Kn} \text{stf } \nabla \mathbf{s}, \quad \Delta := -12 \text{Kn} \nabla \cdot \mathbf{s}.$$

Together, (2.5)–(2.8) form the complete R13 boundary value problem.

2.3. Weak Form. We introduce the following function spaces for the weak form:

$$(2.9) \quad \begin{aligned} \mathbf{T}_\boldsymbol{\sigma} &:= H^1(\Omega; \mathbb{T}), & \mathbf{T}_s &:= H^1(\Omega; \mathbb{R}^d), & \mathbf{T}_p &:= \tilde{H}^1(\Omega), \\ \mathbf{W}_\mathbf{u} &:= L^2(\Omega; \mathbb{R}^d), & \mathbf{W}_\theta &:= L^2(\Omega). \end{aligned}$$

For the sake of analysis, denote by \mathbf{T} and \mathbf{W} composite product Hilbert spaces:

$$(2.10) \quad \mathbf{T} := \mathbf{T}_\boldsymbol{\sigma} \times \mathbf{T}_s \times \mathbf{T}_p, \quad \mathbf{W} := \mathbf{W}_\mathbf{u} \times \mathbf{W}_\theta,$$

together with their canonical norms $\|\cdot\|_T$ and $\|\cdot\|_W$.

Let $(\boldsymbol{\tau}, \mathbf{r}, q, \mathbf{v}, \gamma)$ be the test functions associated with the unknowns $(\boldsymbol{\sigma}, \mathbf{s}, p, \mathbf{u}, \theta)$. We group these into the following tuples:

$$(2.11) \quad \begin{aligned} \text{Unknowns: } \boldsymbol{\mathcal{S}} &:= (\boldsymbol{\sigma}, \mathbf{s}, p) \in T, & \boldsymbol{\mathcal{U}} &:= (\mathbf{u}, \theta) \in W, \\ \text{Test Functions: } \boldsymbol{\mathcal{R}} &:= (\boldsymbol{\tau}, \mathbf{r}, q) \in T, & \boldsymbol{\mathcal{V}} &:= (\mathbf{v}, \gamma) \in W. \end{aligned}$$

The weak formulation is stated as follows: given $\mathcal{F} \in T'$, find $\boldsymbol{\mathcal{S}} \in T$, $\boldsymbol{\mathcal{U}} \in W$ such that

$$(2.12) \quad \begin{aligned} \mathcal{A}(\boldsymbol{\mathcal{S}}, \boldsymbol{\mathcal{R}}) + \mathcal{B}(\boldsymbol{\mathcal{R}}, \boldsymbol{\mathcal{U}}) &= \mathcal{F}(\boldsymbol{\mathcal{R}}) & \forall \boldsymbol{\mathcal{R}} \in T, \\ \mathcal{B}(\boldsymbol{\mathcal{S}}, \boldsymbol{\mathcal{V}}) &= 0 & \forall \boldsymbol{\mathcal{V}} \in W. \end{aligned}$$

Here, the block operators are defined in terms of their constituent forms:

$$(2.13) \quad \begin{cases} \mathcal{A}(\boldsymbol{\mathcal{S}}, \boldsymbol{\mathcal{R}}) := a(\mathbf{s}, \mathbf{r}) + c(\mathbf{s}, \boldsymbol{\tau}) - c(\mathbf{r}, \boldsymbol{\sigma}) + d(\boldsymbol{\sigma}, \boldsymbol{\tau}), \\ \mathcal{B}(\boldsymbol{\mathcal{S}}, \boldsymbol{\mathcal{V}}) := -b(\gamma, \mathbf{s}) - e(\mathbf{v}, \boldsymbol{\sigma}) - g(p, \mathbf{v}), \quad \mathcal{F}(\boldsymbol{\mathcal{R}}) := l_1(\mathbf{r}) + l_2(\boldsymbol{\tau}). \end{cases}$$

The linear functionals, arising from Onsager boundary conditions, are given by

$$(2.14) \quad \begin{cases} l_1(\mathbf{r}) := - \int_{\Gamma} \theta^w r_n dl, \\ l_2(\boldsymbol{\tau}) := - \int_{\Gamma} \sum_{i=1}^2 u_{t_i}^w \tau_{nt_i} dl, \end{cases}$$

and explicit expressions for the bilinear forms are:

$$(2.15) \quad \begin{cases} a(\mathbf{s}, \mathbf{r}) := \frac{24}{25} \text{Kn}(\text{sym} \nabla \mathbf{s}, \text{sym} \nabla \mathbf{r}) + \frac{12}{25} \text{Kn}(\nabla \cdot \mathbf{s}, \nabla \cdot \mathbf{r}) + \frac{4}{15} \frac{1}{\text{Kn}}(\mathbf{s}, \mathbf{r}) \\ \quad + \frac{1}{2} \frac{1}{\tilde{\chi}} \int_{\Gamma} s_n r_n dl + \frac{12}{25} \tilde{\chi} \sum_{i=1}^2 \int_{\Gamma} s_{t_i} r_{t_i} dl, \\ c(\mathbf{r}, \boldsymbol{\sigma}) := \frac{2}{5}(\boldsymbol{\sigma}, \nabla \mathbf{r}) - \frac{3}{20} \int_{\Gamma} \sigma_{nn} r_n dl - \frac{1}{5} \sum_{i=1}^2 \int_{\Gamma} \sigma_{nt_i} r_{t_i} dl, \\ d(\boldsymbol{\sigma}, \boldsymbol{\tau}) := \text{Kn}(\text{Stf} \nabla \boldsymbol{\sigma}, \text{Stf} \nabla \boldsymbol{\tau}) + \frac{1}{2} \frac{1}{\text{Kn}}(\boldsymbol{\sigma}, \boldsymbol{\tau}) + \frac{9}{8} \tilde{\chi} \int_{\Gamma} \sigma_{nn} \tau_{nn} dl \\ \quad + \tilde{\chi} \int_{\Gamma} (\sigma_{t_1 t_1} + \frac{1}{2} \sigma_{nn}) (\tau_{t_1 t_1} + \frac{1}{2} \tau_{nn}) dl + \tilde{\chi} \int_{\Gamma} \sigma_{t_1 t_2} \tau_{t_1 t_2} dl \\ \quad + \frac{1}{\tilde{\chi}} \sum_{i=1}^2 \int_{\Gamma} \sigma_{nt_i} \tau_{nt_i} dl, \\ b(\theta, \mathbf{r}) := (\theta, \nabla \cdot \mathbf{r}), \quad e(\mathbf{u}, \boldsymbol{\tau}) := (\nabla \cdot \boldsymbol{\tau}, \mathbf{u}), \quad g(p, \mathbf{v}) := (\mathbf{v}, \nabla p). \end{cases}$$

For $d = 2$, invoking a symmetry argument allows the function spaces to be simplified via zero-extension of vectors and the natural embedding of tensors:

$$(2.16) \quad \boldsymbol{\sigma} \mapsto \tilde{\boldsymbol{\sigma}} := \begin{bmatrix} \sigma_{11} & \sigma_{12} & 0 \\ \sigma_{12} & \sigma_{22} & 0 \\ 0 & 0 & -(\sigma_{11} + \sigma_{22}) \end{bmatrix}, \quad \boldsymbol{\tau} \mapsto \tilde{\boldsymbol{\tau}} := \begin{bmatrix} \tau_{11} & \tau_{12} & 0 \\ \tau_{12} & \tau_{22} & 0 \\ 0 & 0 & -(\tau_{11} + \tau_{22}) \end{bmatrix},$$

with the corresponding bilinear forms the same as those in [38, Section 3.1].

3. Penalty-free mixed finite elements scheme.

3.1. Finite element spaces and Galerkin formulation. Let \mathcal{T}_h be a conforming triangulation of a domain $\Omega \subset \mathbb{R}^d$ into non-degenerate simplices. We assume that the family of triangulations $\{\mathcal{T}_h\}_{h>0}$ is *shape-regular* and *quasi-uniform* (see [5]). Additionally, for $d = 3$, we impose a mild regularity assumption on the mesh: every tetrahedron must contain at least one vertex in the domain interior to facilitate the analysis. For each element $K \in \mathcal{T}_h$, we denote its diameter by $h_K := \text{diam}(K)$ and define the global mesh size as $h := \max_{K \in \mathcal{T}_h} h_K$.

For any simplex $K \in \mathcal{T}_h$, we denote by $\Delta_l(K)$ the set of its l -dimensional subsimplices for $0 \leq l \leq d$. For instance, $\Delta_d(K) = \{K\}$ consists of the simplex itself, while $\Delta_0(K)$ is the set of its $d+1$ vertices.

We denote by $\mathcal{P}_m(D; \mathbb{X})$ the space of polynomials of degree at most m on a domain D with values in \mathbb{X} . Then the continuous \mathbb{X} -valued Lagrange elements of degree m is defined as $\mathbb{P}_h^m(\Omega; \mathbb{X}) := \{v_h \in H^1(\Omega; \mathbb{X}) : v_h|_K \in \mathcal{P}_m(K; \mathbb{X}) \ \forall K \in \mathcal{T}_h\}$.

On each element $K \in \mathcal{T}_h$, we define the volume bubble function $b_K := \prod_{i=1}^{d+1} \lambda_i$, where λ_i are the barycentric coordinates of K . Let $\mathcal{B}_K^m := \{b_K \mathcal{E}(p) : p \in \mathcal{P}_m(K; \mathbb{R}^d)\}$ denote the local bubble space. For $m \geq d$, we introduce the finite element quintuplet $(\Sigma_h^m, \mathbf{U}_h^m, \mathbf{P}_h^m, \mathbf{S}_h^m, \Theta_h^m)$ defined by:

$$(3.1) \quad \begin{cases} \Sigma_h^m := \{\boldsymbol{\tau}_h \in H^1(\Omega; \mathbb{T}) : \boldsymbol{\tau}_h|_K \in (\mathcal{P}_m(K; \mathbb{T}) \oplus \mathcal{B}_K^m) \ \forall K \in \mathcal{T}_h\}, \\ \mathbf{U}_h^m := \mathbb{P}_h^m(\Omega; \mathbb{R}^d), \quad \mathbf{S}_h^m := \mathbb{P}_h^m(\Omega; \mathbb{R}^d), \\ \mathbf{P}_h^m := \mathbb{P}_h^{m-1}(\Omega) \cap \tilde{H}^1(\Omega), \quad \Theta_h^m := \mathbb{P}_h^{m-1}(\Omega). \end{cases}$$

In the subsequent analysis, we focus on the case $m = d$ for dimensions $d = 2, 3$ and omit the superscript m for brevity. This spatial discretization pairs a bubble-enriched tensor element with two copies of $\mathbb{P}_d \mathbb{P}_{d-1}$ Taylor-Hood elements. Also, we refer to the quintuplet of spaces $(\Sigma_h, \mathbf{U}_h, \mathbf{P}_h, \mathbf{S}_h, \Theta_h)$ as the $\mathbb{P}_d^b \mathbb{P}_d \mathbb{P}_{d-1} \mathbb{P}_d \mathbb{P}_{d-1}$ element.

Remark 3.1 (Necessity for $m \geq d$). The condition $m \geq d$ is sufficient to ensure the existence of a trivial right inverse of the divergence operator in Σ_h^m for $\ker(\mathcal{E})$. As detailed in Lemma 3.6, this kernel satisfies the inclusion $\mathcal{P}_{d-2} \subsetneq \ker(\mathcal{E}) \subsetneq \mathcal{P}_{d-1}$.

Remark 3.2 (Why 2D). While $d = 2$ can be viewed as a special case of $d = 3$, adopting this perspective would impose the restriction $m \geq 3$ required by the 3D analysis. This would preclude the use of the lowest-order element ($m = 2$) in two dimensions. Given the significant expense associated with higher-order elements, we focus primarily on the minimal case $m = d$. Nevertheless, the proposed scheme is readily extensible to $m > d$ for higher orders of convergence.

Let $(\boldsymbol{\tau}_h, \mathbf{r}_h, q_h, \mathbf{v}_h, \gamma_h)$ denote the test functions corresponding to solution fields $(\boldsymbol{\sigma}_h, \mathbf{s}_h, p_h, \mathbf{u}_h, \theta_h)$, respectively. For simplicity, we define

$$(3.2) \quad \begin{aligned} \text{Galerkin Solutions:} \quad & \boldsymbol{\mathcal{S}}_h := (\boldsymbol{\sigma}_h, \mathbf{s}_h, p_h) \in \mathbf{T}_h, \quad \boldsymbol{\mathcal{U}}_h := (\mathbf{u}_h, \theta_h) \in \mathbf{W}_h, \\ \text{Discrete Test Functions:} \quad & \boldsymbol{\mathcal{R}}_h := (\boldsymbol{\tau}_h, \mathbf{r}_h, q_h) \in \mathbf{T}_h, \quad \boldsymbol{\mathcal{V}}_h := (\mathbf{v}_h, \gamma_h) \in \mathbf{W}_h, \end{aligned}$$

where $\mathbf{T}_h := \Sigma_h \times \mathbf{U}_h \times \mathbf{P}_h$, $\mathbf{W}_h := \mathbf{U}_h \times \Theta_h$. Then the Galerkin formulation reads: find $\boldsymbol{\mathcal{S}}_h \in \mathbf{T}_h$, $\boldsymbol{\mathcal{U}}_h \in \mathbf{W}_h$ such that

$$(3.3) \quad \begin{aligned} \mathcal{A}(\boldsymbol{\mathcal{S}}_h, \boldsymbol{\mathcal{R}}_h) + \mathcal{B}(\boldsymbol{\mathcal{R}}_h, \boldsymbol{\mathcal{U}}_h) &= \mathcal{F}(\boldsymbol{\mathcal{R}}_h) \quad \forall \boldsymbol{\mathcal{R}}_h \in \mathbf{T}_h, \\ \mathcal{B}(\boldsymbol{\mathcal{S}}_h, \boldsymbol{\mathcal{V}}_h) &= 0 \quad \forall \boldsymbol{\mathcal{V}}_h \in \mathbf{W}_h. \end{aligned}$$

3.2. Bubble-enriched element space and interpolation operator. Following [1], the local degrees of freedom (DoFs) for Σ_h on K are defined by

$$(3.4) \quad \begin{aligned} \boldsymbol{\tau}(\delta), \quad & \forall \delta \in \Delta_0(K), \\ (\boldsymbol{\tau}, \boldsymbol{\sigma})_f, \quad & \forall \boldsymbol{\sigma} \in \mathcal{P}_{d-(r+1)}(f; \mathbb{T}), f \in \Delta_r(K), r = 1, \dots, d-1, \\ (\boldsymbol{\tau}, \boldsymbol{\sigma})_K, \quad & \forall \boldsymbol{\sigma} \in \mathcal{EP}_d(K; \mathbb{R}^d). \end{aligned}$$

The unisolvence of (3.4) is established in [1, Lemma 2.1].

Notably, these DoFs induce an H^1 -stable interpolator that preserves homogeneous traces for non-smooth tensor fields. Define the subspace with homogeneous boundary

conditions as $\Sigma_{h,0} := \Sigma_h \cap H_0^1(\Omega; \mathbb{T})$. Let $Q_K : L^2(K; \mathbb{T}) \rightarrow \mathcal{P}_d(K; \mathbb{T}) \oplus \mathcal{B}_K$ be the local L^2 -orthogonal projection operator on K . The interpolation operator $\mathcal{I}_h : H_0^1(\Omega; \mathbb{T}) \rightarrow \Sigma_{h,0}$ is uniquely determined by:

$$(3.5) \quad \begin{aligned} \mathcal{I}_h \boldsymbol{\tau}(\delta) &:= \frac{1}{\#\mathcal{T}_\delta} \sum_{K \in \mathcal{T}_\delta} (Q_K \boldsymbol{\tau})(\delta), \\ (\mathcal{I}_h \boldsymbol{\tau}, \boldsymbol{\sigma})_f &:= \frac{1}{\#\mathcal{T}_f} \sum_{K \in \mathcal{T}_f} (Q_K \boldsymbol{\tau}, \boldsymbol{\sigma})_f \quad \forall \boldsymbol{\sigma} \in \mathcal{P}_{k-(r+1)}(f; \mathbb{T}), \\ (\mathcal{I}_h \boldsymbol{\tau}, \boldsymbol{\sigma})_K &:= (\boldsymbol{\tau}, \boldsymbol{\sigma})_K \quad \forall \boldsymbol{\sigma} \in \mathcal{E}(\mathcal{P}_d(K; \mathbb{R}^d)), \end{aligned}$$

for all interior vertices δ , interior r -dimensional sub-simplices f ($r = 1, \dots, d-1$) and d -dimensional simplex elements K of \mathcal{T}_h . Here, \mathcal{T}_δ and \mathcal{T}_f denote the sets of elements in \mathcal{T}_h sharing the vertex δ or the sub-simplex f , respectively. Analogous to [1, Lemma 2.2], this operator satisfies the following stability and approximation properties:

LEMMA 3.3. *The interpolation operator $\mathcal{I}_h : H_0^1(\Omega; \mathbb{T}) \rightarrow \Sigma_{h,0}$ defined by (3.5) is H^1 -stable and preserves the homogeneous trace. It has the following properties:*

- (Homogeneous trace preservation) $\mathcal{I}_h(H_0^1(\Omega; \mathbb{T})) \subseteq H_0^1(\Omega; \mathbb{T})$,
- (H^1 -stability) $\|\mathcal{I}_h \boldsymbol{\tau}\|_1 \lesssim |\boldsymbol{\tau}|_1$,
- (L^2 -approximation property) $\|\boldsymbol{\tau} - \mathcal{I}_h \boldsymbol{\tau}\|_0 \lesssim h|\boldsymbol{\tau}|_1$,
- (H^1 -approximation property) $|\boldsymbol{\tau} - \mathcal{I}_h \boldsymbol{\tau}|_1 \lesssim |\boldsymbol{\tau}|_1$.

Remark 3.4. For the case $d = 2$, Lemma 3.3 corresponds to the result established in [1, Lemma 2.2]; a detailed proof is also provided in our supplementary material. For $d = 3$, the result follows from analogous arguments, noting that the space of symmetric trace-free tensors is a subspace of the space of symmetric tensors.

3.3. Kernel space and orthogonal decomposition. To establish a unified framework for both two- and three-dimensional cases, we begin by characterizing the kernel of \mathcal{E} and deriving an orthogonal decomposition of the discrete space \mathbf{U}_h .

Denote by \mathcal{K} the kernel of \mathcal{E} in $L^2(\Omega; \mathbb{R}^d)$ in the distributional sense:

$$(3.6) \quad \mathcal{K} := \ker(\mathcal{E}) = \{\mathbf{v} \in L^2(\Omega; \mathbb{R}^d) \mid \mathcal{E}\mathbf{v} = \mathbf{0}\}.$$

We now present a series of lemmas characterizing the properties of \mathcal{E} and \mathcal{K} .

LEMMA 3.5 (Adjoint Operator). *The operator $\mathcal{E} : L^2(\Omega; \mathbb{R}^d) \rightarrow H^{-1}(\Omega; \mathbb{T})$ is the adjoint of divergence operator $-\nabla \cdot : H_0^1(\Omega; \mathbb{T}) \rightarrow L^2(\Omega; \mathbb{R}^d)$, i.e., $-\nabla \cdot = (\mathcal{E})'$.*

Proof. Let $\mathbf{v} \in L^2(\Omega; \mathbb{R}^d)$ and $\boldsymbol{\tau} \in H_0^1(\Omega; \mathbb{T})$. A key observation is that the gradient $\nabla \mathbf{v}$ can be decomposed as $\nabla \mathbf{v} = \mathcal{E}\mathbf{v} + (\nabla \mathbf{v} - \mathcal{E}\mathbf{v})$.

By the definitions of \mathcal{E} and \mathbb{T} , the second term $(\nabla \mathbf{v} - \mathcal{E}\mathbf{v})$ is orthogonal to any tensor in \mathbb{T} with respect to the Frobenius inner product. For $d = 2$, $\nabla \mathbf{v} - \mathcal{E}\mathbf{v} = \text{skew}(\nabla \mathbf{v})$, which is orthogonal to the symmetric tensor $\boldsymbol{\tau}$. For $d = 3$, $\nabla \mathbf{v} - \mathcal{E}\mathbf{v}$ is a sum of a skew-symmetric and a pure trace tensor, both of which are orthogonal to the symmetric and trace-free tensor $\boldsymbol{\tau}$. Thus, in both cases, we have $(\mathcal{E}\mathbf{v}, \boldsymbol{\tau}) = (\nabla \mathbf{v}, \boldsymbol{\tau})$.

Using this identity and integration by parts, we obtain

$$(3.7) \quad \langle \mathcal{E}\mathbf{v}, \boldsymbol{\tau} \rangle_{H^{-1}, H_0^1} = (\mathcal{E}\mathbf{v}, \boldsymbol{\tau}) = (\nabla \mathbf{v}, \boldsymbol{\tau}) = -(\mathbf{v}, \nabla \cdot \boldsymbol{\tau}),$$

which completes the proof. \square

Next, we characterize the kernel of the operator \mathcal{E} .

LEMMA 3.6 (Characterization of the Kernel). *The kernel of \mathcal{E} in the distributional sense, $\mathcal{K} := \ker(\mathcal{E}|_{L^2})$, is a finite-dimensional space of polynomials. Specifically:*

- For $d = 2$, \mathcal{K} is the space of rigid motions \mathbf{RM} , which are affine maps of the form $\mathbf{v}(\mathbf{x}) = \mathbf{a} + A\mathbf{x}$ where $\mathbf{a} \in \mathbb{R}^2$ and $A \in \mathbb{R}^{2 \times 2}$ is a skew-symmetric matrix. These are polynomials of degree at most one, leading to $\mathcal{P}_0 \subsetneq \mathbf{RM} \subsetneq \mathcal{P}_1$.
- For $d = 3$, \mathcal{K} is the space of conformal Killing maps \mathbf{CK} composed of

$$(3.8) \quad \mathbf{v}(\mathbf{x}) = \mathbf{a} + \lambda\mathbf{x} + A\mathbf{x} + (2(\mathbf{b} \cdot \mathbf{x})\mathbf{x} - \|\mathbf{x}\|^2\mathbf{b}),$$

for some constants $\mathbf{a}, \mathbf{b} \in \mathbb{R}^3$, $\lambda \in \mathbb{R}$, and a skew-symmetric matrix $A \in \mathbb{R}^{3 \times 3}$. These are polynomials of degree at most two, leading to $\mathcal{P}_1 \subsetneq \mathbf{CK} \subsetneq \mathcal{P}_2$.

Proof. For a rigorous proof, see, e.g., [11, Theorem 2.2] for \mathbf{RM} and [28, Proposition 2.5] for \mathbf{CK} . \square

Let $\mathbf{Y} \subset L^2(\Omega; \mathbb{R}^d)$ be a finite-dimensional space, for instance, $\mathbb{P}_h^k(\Omega; \mathbb{R}^d)$. The next lemma shows that if \mathbf{Y} is sufficiently rich, its kernel under \mathcal{E} is precisely \mathcal{K} .

LEMMA 3.7 (Invariance of the Kernel). *Let \mathbf{Y} be a finite-dimensional subspace of $L^2(\Omega; \mathbb{R}^d)$ such that $\mathcal{K} \subseteq \mathbf{Y}$. Then the kernel of \mathcal{E} restricted to \mathbf{Y} coincides with \mathcal{K} .*

Proof. By definition, $\mathcal{K} = \ker(\mathcal{E}|_{L^2})$. The inclusion $\mathcal{K} \subseteq \ker(\mathcal{E}|_{\mathbf{Y}})$ is immediate from the assumption $\mathcal{K} \subseteq \mathbf{Y}$. The converse direction is also obvious. \square

This result allows for a unique orthogonal decomposition of both the continuous space $L^2(\Omega; \mathbb{R}^d)$ and the discrete space $\mathbf{U}_h = \mathbb{P}_h^d(\Omega; \mathbb{R}^d)$ with respect to the kernel \mathcal{K} . Let \mathcal{K}^\perp be the orthogonal complement of \mathcal{K} in $L^2(\Omega; \mathbb{R}^d)$. By taking $\mathbf{Y} = \mathbf{U}_h$, we have the following L^2 -orthogonal decompositions:

$$(3.9) \quad L^2(\Omega; \mathbb{R}^d) = \mathcal{K} \oplus \mathcal{K}^\perp, \quad \mathbf{U}_h = \mathcal{K} \oplus \mathbf{U}_{h,0},$$

where the orthogonal complement of \mathcal{K} within the subspace \mathbf{U}_h is denoted as $\mathbf{U}_{h,0}$,

$$(3.10) \quad \mathbf{U}_{h,0} := \mathcal{K}^\perp \cap \mathbf{U}_h.$$

LEMMA 3.8. *The space $\mathbf{U}_{h,0}$ is a closed subspace of \mathcal{K}^\perp .*

Proof. By definition, $\mathbf{U}_{h,0} = \mathcal{K}^\perp \cap \mathbf{U}_h$. Since \mathcal{K} is a subset of the Hilbert space $L^2(\Omega; \mathbb{R}^d)$, its orthogonal complement \mathcal{K}^\perp is a closed subspace. As a finite-dimensional subspace of a normed space, \mathbf{U}_h is closed. Hence $\mathbf{U}_{h,0}$ is a closed subspace in \mathcal{K}^\perp . \square

Finally, we point out that \mathcal{I}_h is B -compatible for $\mathbf{U}_{h,0}$.

LEMMA 3.9 (B -Compatibility). $\forall \mathbf{u}_h \in \mathbf{U}_{h,0}$, $(\nabla \cdot (\boldsymbol{\tau} - \mathcal{I}_h \boldsymbol{\tau}), \mathbf{u}_h) = 0$.

Proof. Since $\boldsymbol{\tau} - \mathcal{I}_h \boldsymbol{\tau} \in H_0^1(\Omega; \mathbb{T})$, Lemma 3.5 and the definition of \mathcal{I}_h yield

$$(3.11) \quad (\nabla \cdot (\boldsymbol{\tau} - \mathcal{I}_h \boldsymbol{\tau}), \mathbf{u}_h)_K = -(\boldsymbol{\tau} - \mathcal{I}_h \boldsymbol{\tau}, \mathcal{E} \mathbf{u}_h)_K = 0$$

for each element $K \in \mathcal{T}_h$. \square

4. Stability and convergence. In this section, we establish the stability of the penalty-free MFEM scheme and the order of convergence under certain mild regularity assumptions. The unisolvence of MFEM is established via coercivity on the kernel and the inf-sup condition:

1. *Coercivity on discrete kernel.* Let $\ker B_h := \{\mathbf{S}_h \in \mathbf{T}_h : \mathcal{B}(\mathbf{S}_h, \mathbf{V}_h) = 0, \forall \mathbf{V}_h \in \mathbf{W}_h\}$. Coercivity requires $\mathcal{A}(\mathbf{S}_h, \mathbf{S}_h) \gtrsim \|\mathbf{S}_h\|^2$ for all $\mathbf{S}_h \in \ker B_h$. By derivation, it suffices to show that for any $(\boldsymbol{\sigma}_h, \mathbf{s}_h, p_h) \in \ker B_h$,

(U-1)

$$\|\operatorname{sym} \nabla \mathbf{s}_h\|_0^2 + \|\mathbf{s}_h\|_0^2 + \|\operatorname{Stf} \nabla \boldsymbol{\sigma}_h\|_0^2 + \|\boldsymbol{\sigma}_h\|_0^2 \gtrsim \|\mathbf{s}_h\|_1^2 + \|\boldsymbol{\sigma}_h\|_1^2 + \|p_h\|_1^2.$$

2. *Discrete inf-sup condition.* The discrete stability condition for $(\mathbf{T}_h, \mathbf{W}_h)$,

$$(4.1) \quad \inf_{\mathbf{v}_h \in \mathbf{W}_h} \sup_{\boldsymbol{\sigma}_h \in \mathbf{T}_h} \frac{-(\mathbf{v}_h, \nabla \cdot \boldsymbol{\sigma}_h) - (\nabla p_h, \mathbf{v}_h) - (\gamma_h, \nabla \cdot \mathbf{s}_h)}{(\|\boldsymbol{\sigma}_h\|_1^2 + \|\mathbf{s}_h\|_1^2 + \|p_h\|_1^2)^{1/2} (\|\mathbf{v}_h\|_0^2 + \|\gamma_h\|_0^2)^{1/2}} \gtrsim 1$$

is satisfied provided the decoupled conditions hold for all $\mathbf{v}_h \in \mathbf{U}_h$, $\gamma_h \in \Theta_h$:

$$(U-2) \quad \sup_{\boldsymbol{\sigma}_h \in \Sigma_h} \frac{-(\mathbf{v}_h, \nabla \cdot \boldsymbol{\sigma}_h)}{\|\boldsymbol{\sigma}_h\|_1} \gtrsim \|\mathbf{v}_h\|_0, \quad \sup_{\mathbf{s}_h \in \mathbf{S}_h} \frac{-(\gamma_h, \nabla \cdot \mathbf{s}_h)}{\|\mathbf{s}_h\|_1} \gtrsim \|\gamma_h\|_0.$$

These decoupled conditions ensure the existence of non-trivial $(\boldsymbol{\sigma}_h, \mathbf{s}_h) \in \Sigma_h \times \mathbf{S}_h$ satisfying the following stability estimates with constants $C_1, C_2 > 0$:

$$-(\mathbf{v}_h, \nabla \cdot \boldsymbol{\sigma}_h) \geq C_1 \|\mathbf{v}_h\|_0 \|\boldsymbol{\sigma}_h\|_1, \quad -(\gamma_h, \nabla \cdot \mathbf{s}_h) \geq C_2 \|\gamma_h\|_0 \|\mathbf{s}_h\|_1.$$

Then constructing $\mathcal{S}_h = (\boldsymbol{\sigma}_h, \mathbf{s}_h, 0) \in \mathbf{T}_h$ and scaling the components such that $\|\boldsymbol{\sigma}_h\|_1 = C_1 \|\mathbf{v}_h\|_0$ and $\|\mathbf{s}_h\|_1 = C_2 \|\gamma_h\|_0$ yield

$$(4.2) \quad \sup_{\mathcal{S}_h \in \mathbf{T}_h} \frac{\mathcal{B}(\mathcal{S}_h, \mathbf{V}_h)}{\|\mathcal{S}_h\|_{\mathbf{T}}} \geq \sqrt{\|\boldsymbol{\sigma}_h\|_1^2 + \|\mathbf{s}_h\|_1^2} \gtrsim \sqrt{\|\mathbf{v}_h\|_0^2 + \|\gamma_h\|_0^2} = \|\mathbf{V}_h\|_{\mathbf{W}},$$

thereby verifying the joint discrete inf-sup condition.

4.1. Discrete inf-sup condition. For the relatively simple pair (\mathbf{S}_h, Θ_h) from decoupled inf-sup conditions (U-2), the stability of this $\mathbb{P}_d\mathbb{P}_{d-1}$ pair relies on the discrete inf-sup condition for the Stokes equations with pure Neumann boundary conditions. This is usually viewed as a natural corollary of the Dirichlet case. However, as we have not located an explicit reference for our specific formulation, we briefly sketch the proof, employing Verfürth's argument.

THEOREM 4.1. *The finite element spaces (\mathbf{S}_h, Θ_h) satisfy the discrete inf-sup condition,*

$$(4.3) \quad \sup_{\mathbf{s}_h \in \mathbf{S}_h} \frac{(\gamma_h, \nabla \cdot \mathbf{s}_h)}{\|\mathbf{s}_h\|_1} \gtrsim \|\gamma_h\|_0, \quad \forall \gamma_h \in \Theta_h.$$

Proof. Decompose the temperature space according to $\Theta_h = \Theta_{h,0} \oplus \mathbb{R}$ such that $\Theta_{h,0}$ is zero-mean space. For any $\gamma_h \in \Theta_h$, we write $\gamma_h = \gamma_{h,0} + \hat{\gamma}$ correspondingly.

We first show that for $\gamma_h \in \Theta_h$, there exists $\mathbf{r}_h \in \mathbf{S}_h$ with $\|\mathbf{r}_h\|_1 \lesssim \|\gamma_h\|_0$ and

$$(4.4) \quad (\gamma_h, \nabla \cdot \mathbf{r}_h) \gtrsim \|\gamma_h\|_0^2 - h \|\gamma_h\|_0 \|\nabla \gamma_h\|_0 \gtrsim \|\mathbf{r}_h\|_1 (\|\gamma_h\|_0 - h \|\nabla \gamma_h\|_0).$$

For the zero-mean component $\gamma_{h,0}$, there exists $\mathbf{r}_0 \in H_0^1(\Omega; \mathbb{R}^d)$ such that $\nabla \cdot \mathbf{r}_0 = \gamma_{h,0}$ with $\|\mathbf{r}_0\|_1 \lesssim \|\gamma_{h,0}\|_0$, which follows from the existence of a right inverse for divergence (see, e.g., [4, Theorem IV.3.1]). Then denote by $\mathbf{r}_{h,0}$ the Scott-Zhang interpolation of \mathbf{r}_0 into $\mathbf{S}_h \cap H_0^1$ (see [29]). And for the constant term, let $\hat{\mathbf{r}} = \hat{\gamma} \mathbf{x}/d$ with $\nabla \cdot \hat{\mathbf{r}} = \hat{\gamma}$. Therefore, picking $\mathbf{r}_h := \mathbf{r}_{h,0} + \hat{\mathbf{r}}$ and applying the approximation property of the Scott-Zhang interpolation $\|\mathbf{r}_0 - \mathbf{r}_{h,0}\|_0 \lesssim h \|\mathbf{r}_0\|_1$ yield (4.4).

By the same arguments as given in [7, 31], the stability of Taylor-Hood elements under Dirichlet boundary conditions ensures there exists $\mathbf{s}_{h,0} \in (\mathbf{S}_h \cap H_0^1)$ such that

$$(4.5) \quad (\gamma_h, \nabla \cdot \mathbf{s}_{h,0}) \gtrsim h \|\mathbf{s}_{h,0}\|_1 \|\nabla \gamma_h\|_0.$$

Combining (4.4) and (4.5) completes the proof. \square

As for the \mathbb{P}_d^b - \mathbb{P}_d pair (Σ_h, \mathbf{U}_h) , previous numerical experiments (e.g., [44, Section 3]) showed that the standard Taylor-Hood element pair doesn't work well and some penalty terms are needed to ensure the numerical stability. Here, our approach is to enrich Lagrange element spaces with volume bubble functions as a conforming stabilization. The main issue is then to verify for any $\mathbf{u}_h \in \mathbf{U}_h$,

$$\sup_{\boldsymbol{\sigma}_h \in \Sigma_h} \frac{(\nabla \cdot \boldsymbol{\sigma}_h, \mathbf{u}_h)}{\|\boldsymbol{\sigma}_h\|_1} \gtrsim \|\mathbf{u}_h\|_0.$$

While one might ideally define $\boldsymbol{\sigma}_h = (\nabla \cdot)^{-1}(\mathbf{u}_h)$ while preserving H^1 stability, such a construction is difficult to realize in the discrete setting. We therefore pursue an alternative strategy, inspired by the proof of Theorem 4.1 and centered on orthogonal decompositions (3.9). Our first step involves demonstrating the existence of a right inverse for the divergence operator, restricted to the orthogonal complement of its adjoint's kernel \mathcal{K}^\perp .

THEOREM 4.2 (Existence of right inverse for the divergence operator). *For $\mathbf{u} \in \mathcal{K}^\perp$, there exists $\boldsymbol{\tau} \in H_0^1(\Omega; \mathbb{T})$ such that*

$$(4.6) \quad -\nabla \cdot \boldsymbol{\tau} = \mathbf{u}, \quad \|\boldsymbol{\tau}\|_1 \lesssim \|\mathbf{u}\|_0.$$

Proof. For the $d = 2$ case, we show the divergence operator is a surjective map from $H_0^1(\Omega; \mathbb{R}_{\text{sym}}^{2 \times 2})$ to \mathbf{RM}^\perp . By Lemma 3.5, the adjoint of $-\text{div}$ is $\text{sym } \nabla : L^2(\Omega; \mathbb{R}^2) \rightarrow H^{-1}(\Omega; \mathbb{R}_{\text{sym}}^{2 \times 2})$, and the kernel of the adjoint is the space of rigid motions, \mathbf{RM} . According to the closed range theorem, if the range of the adjoint operator $\text{sym } \nabla$ is closed in $H^{-1}(\Omega; \mathbb{R}_{\text{sym}}^{2 \times 2})$, then the range of the primal operator $-\text{div}$ equals the orthogonal complement of the adjoint's kernel, that is

$$(4.7) \quad \text{Range}(\text{div}) = (\ker(\text{sym } \nabla))^\perp = \mathbf{RM}^\perp.$$

To show $\text{Range}(\text{sym } \nabla)$ is closed, it suffices to verify that $\text{sym } \nabla$ is bounded below on the orthogonal complement of its kernel, that is, for all $\mathbf{v} \in \mathbf{RM}^\perp \subseteq L^2(\Omega; \mathbb{R}^2)$,

$$(4.8) \quad \|\text{sym } \nabla \mathbf{v}\|_{-1} \gtrsim \|\mathbf{v}\|_0.$$

The above inequality follows from Korn's inequality of negative norm (see e.g., [14, Theorem 3.2]), which states:

$$(4.9) \quad \|\mathbf{v}\|_0 \lesssim \|\text{sym } \nabla \mathbf{v}\|_{-1} + \|\mathbf{v}\|_{-1}, \quad \forall \mathbf{v} \in L^2(\Omega; \mathbb{R}^2).$$

Assume for the sake of contradiction that (4.8) fails. Then there exists a sequence $\{\mathbf{v}_k\} \subset \mathbf{RM}^\perp$ with $\|\mathbf{v}_k\|_0 = 1$ such that $\|\text{sym } \nabla \mathbf{v}_k\|_{-1} \rightarrow 0$. Since the embedding $L^2(\Omega) \hookrightarrow H^{-1}(\Omega)$ is compact on bounded Lipschitz domain, there exists a subsequence convergent under H^{-1} norm, which means

$$\|\mathbf{v}_{k_n} - \mathbf{v}_{k_m}\|_{-1} \rightarrow 0$$

as $n, m \rightarrow \infty$. By the Korn's inequality (4.9) applied to $\mathbf{v}_{k_n} - \mathbf{v}_{k_m}$, such subsequence is also Cauchy sequence under L^2 norm. Then let \mathbf{v}^* be the limit under the L^2 norm. We have $\|\mathbf{v}^*\|_0 = 1$, $\mathbf{v}^* \in \mathbf{RM}^\perp$, and continuity implies $\text{sym } \nabla \mathbf{v}^* = 0$. Thus $\mathbf{v}^* \in \mathbf{RM}$, which implies $\mathbf{v}^* = 0$, a contradiction.

Hence, the range of $\text{sym } \nabla$ is closed and the operator $-\text{div} : H_0^1(\Omega; \mathbb{R}_{\text{sym}}^{2 \times 2}) \rightarrow \mathbf{RM}^\perp$ is surjective. Since the open mapping theorem guarantees the existence of a continuous right inverse, for any $\mathbf{u} \in \mathbf{RM}^\perp$, consequently there exists $\boldsymbol{\tau} \in H_0^1(\Omega; \mathbb{R}_{\text{sym}}^{2 \times 2})$ satisfying $-\nabla \cdot \boldsymbol{\tau} = \mathbf{u}$ such that $\|\boldsymbol{\tau}\|_1 \lesssim \|\mathbf{u}\|_0$.

The proof for the $d = 3$ case follows an identical logic to that for $d = 2$ with **RM** replaced by **CK** and relies on a generalized Korn's inequality of negative norm,

$$\|\mathbf{v}\|_0 \lesssim \|\text{stf } \nabla \mathbf{v}\|_{-1} + \|\mathbf{v}\|_{-1}.$$

A detailed proof for the above inequality is provided in Theorem A.4. \square

Therefore, combining Lemma 3.8 and Theorem 4.2 yields:

THEOREM 4.3. *For $\mathbf{u}_h \in \mathbf{U}_{h,0}$, there exists $\boldsymbol{\tau}_h \in H_0^1(\Omega; \mathbb{T})$ such that*

$$(4.10) \quad -\nabla \cdot \boldsymbol{\tau}_h = \mathbf{u}_h, \quad \|\boldsymbol{\tau}_h\|_1 \lesssim \|\mathbf{u}_h\|_0.$$

Now we turn to our case and derive the discrete inf-sup condition for the $\mathbb{P}_d^b\mathbb{P}_d$ pair (Σ_h, \mathbf{U}_h) . The proof is also based on a useful lemma related to the trivial right inverse of divergence in Σ_h acting on \mathcal{K} , another component of \mathbf{U}_h .

LEMMA 4.4. *For $\hat{\mathbf{u}} \in \mathcal{K}$, there exists $\hat{\boldsymbol{\sigma}} \in \Sigma_h$ such that $\hat{\mathbf{u}} = \nabla \cdot \hat{\boldsymbol{\sigma}}$, $\|\hat{\boldsymbol{\sigma}}\|_1 \lesssim \|\hat{\mathbf{u}}\|_0$.*

Proof. For $d = 2$, a rigid body motion $\hat{\mathbf{u}}$ writes as:

$$\hat{\mathbf{u}} = (ax_2 + b_1, -ax_1 + b_2) = a(x_2 \mathbf{e}_1 - x_1 \mathbf{e}_2) + b_1 \mathbf{e}_1 + b_2 \mathbf{e}_2.$$

Construct $\hat{\boldsymbol{\sigma}} = (ax_1 x_2 + b_1 x_1) \mathbf{e}_1 \otimes \mathbf{e}_1 + (-ax_1 x_2 + b_2 x_2) \mathbf{e}_2 \otimes \mathbf{e}_2 \in \mathcal{P}_2 \subseteq \Sigma_h$. A direct calculation of the divergence gives $\nabla \cdot \hat{\boldsymbol{\sigma}} = \hat{\mathbf{u}}$.

Also, note that $\|\hat{\mathbf{u}}\|_0$ can be viewed as a norm on \mathbb{R}^3 , let's say, $\|\cdot\|_{\hat{\mathbf{u}}} : \mathbb{R}^3 \rightarrow \mathbb{R}$ induced by $\|(a, b, c)\|_{\hat{\mathbf{u}}} := \|\hat{\mathbf{u}}\|_0 = \|(ax_2 + b, -ax_1 + c)\|_0$. We claim $\|\cdot\|_{\hat{\mathbf{u}}}$ is a norm. The homogeneity and positive definiteness are obvious. For triangle inequality,

$$\begin{aligned} \|(a_1, b_1, c_1) + (a_2, b_2, c_2)\|_{\hat{\mathbf{u}}} &= \|\hat{\mathbf{u}}_1 + \hat{\mathbf{u}}_2\|_0 \\ &\leq \|\hat{\mathbf{u}}_1\|_0 + \|\hat{\mathbf{u}}_2\|_0 = \|(a_1, b_1, c_1)\|_{\hat{\mathbf{u}}} + \|(a_2, b_2, c_2)\|_{\hat{\mathbf{u}}}. \end{aligned}$$

Hence $\|\cdot\|_{\hat{\mathbf{u}}}$ is a norm on \mathbb{R}^3 . Similarly, $\|\hat{\boldsymbol{\sigma}}\|_1$ can induce $\|(a, b, c)\|_{\hat{\boldsymbol{\sigma}}} := \|\hat{\boldsymbol{\sigma}}\|_1$ as a norm on \mathbb{R}^3 and applying the equivalence of norms in \mathbb{R}^3 completes the proof.

For $d = 3$, since **CK** $\subseteq \mathcal{P}_2(\Omega; \mathbb{R}^3)$ is a finite-dimensional space of polynomials, for any $\hat{\mathbf{u}} \in \mathbf{CK}$, it suffices to construct a polynomial tensor $\hat{\boldsymbol{\sigma}} \in \mathcal{P}_3(\Omega; \mathbb{R}_{\text{stf}}^{3 \times 3})$ such that $\nabla \cdot \hat{\boldsymbol{\sigma}} = \hat{\mathbf{u}}$. Note that any $\hat{\mathbf{u}} \in \mathbf{CK}$ can be decomposed into four different parts:

$$(4.11) \quad \hat{\mathbf{u}}(\mathbf{x}) = \underbrace{\mathbf{a}}_{\text{Translation}} + \underbrace{A\mathbf{x}}_{\text{Rotation}} + \underbrace{\lambda \mathbf{x}}_{\text{Scaling}} + \underbrace{(2(\mathbf{b} \cdot \mathbf{x})\mathbf{x} - \|\mathbf{x}\|^2 \mathbf{b})}_{\text{Special Conformal}}.$$

We construct $\hat{\boldsymbol{\sigma}} \in \mathcal{P}_3(\Omega; \mathbb{R}_{\text{stf}}^{3 \times 3}) \subseteq \Sigma_h$ for each type $\hat{\mathbf{u}}$ such that $\nabla \cdot \hat{\boldsymbol{\sigma}} = \hat{\mathbf{u}}$ as follows:

- For translation motion $\hat{\mathbf{u}} = \mathbf{a}$, define $\hat{\boldsymbol{\sigma}} = (3(\mathbf{a} \otimes \mathbf{x} + \mathbf{x} \otimes \mathbf{a}) - 2(\mathbf{a} \cdot \mathbf{x})\mathbf{I})/10$.
- For rotation motion $\hat{\mathbf{u}} = A\mathbf{x}$, define $\hat{\boldsymbol{\sigma}} = ((A\mathbf{x}) \otimes \mathbf{x} + \mathbf{x} \otimes (A\mathbf{x}))/5$.
- For scaling motion $\hat{\mathbf{u}} = \lambda \mathbf{x}$, define $\hat{\boldsymbol{\sigma}} = 3\lambda(\mathbf{x} \otimes \mathbf{x} - \frac{1}{3}\|\mathbf{x}\|^2 \mathbf{I})/10$.
- For special conformal motion $\hat{\mathbf{u}} = 2(\mathbf{b} \cdot \mathbf{x})\mathbf{x} - \|\mathbf{x}\|^2 \mathbf{b}$, define

$$\hat{\boldsymbol{\sigma}} = \frac{1}{70} (34(\mathbf{b} \cdot \mathbf{x})\mathbf{x} \otimes \mathbf{x} - 11\|\mathbf{x}\|^2(\mathbf{b} \otimes \mathbf{x} + \mathbf{x} \otimes \mathbf{b}) - 4\|\mathbf{x}\|^2(\mathbf{b} \cdot \mathbf{x})\mathbf{I}).$$

Then applying the equivalence of norms in finite-dimensional spaces, as in the proof of $d = 2$, completes the proof. \square

We come to the discrete inf-sup condition for (Σ_h, \mathbf{U}_h) at the end of this subsection:

THEOREM 4.5. *The finite element spaces (Σ_h, \mathbf{U}_h) satisfy the discrete inf-sup condition,*

$$(4.12) \quad \inf_{\mathbf{u}_h \in \mathbf{U}_h} \sup_{\boldsymbol{\sigma}_h \in \Sigma_h} \frac{(\mathbf{u}_h, \nabla \cdot \boldsymbol{\sigma}_h)}{\|\mathbf{u}_h\|_0 \|\boldsymbol{\sigma}_h\|_1} \gtrsim 1.$$

Proof. Any given $\mathbf{u}_h \in \mathbf{U}_h$ admits the decomposition:

$$(4.13) \quad \mathbf{u}_h = \mathbf{u}_{h,0} + \hat{\mathbf{u}}, \quad \mathbf{u}_{h,0} \in \mathbf{U}_{h,0}, \quad \hat{\mathbf{u}} \in \mathcal{K}.$$

By Theorem 4.3, there exists $\boldsymbol{\sigma}_0 \in H_0^1(\Omega; \mathbb{T})$ such that,

$$(4.14) \quad \nabla \cdot \boldsymbol{\sigma}_0 = \mathbf{u}_{h,0}, \quad \|\boldsymbol{\sigma}_0\|_1 \lesssim \|\mathbf{u}_{h,0}\|_0.$$

Denote $\boldsymbol{\sigma}_{h,0} := \mathcal{I}_h \boldsymbol{\sigma}_0 \in \Sigma_{h,0}$ where the interpolation operator \mathcal{I}_h is defined in (3.5). Also, by Lemma 4.4, there exists $\hat{\boldsymbol{\sigma}} \in \Sigma_h$ such that,

$$(4.15) \quad \nabla \cdot \hat{\boldsymbol{\sigma}} = \hat{\mathbf{u}}, \quad \|\hat{\boldsymbol{\sigma}}\|_1 \lesssim \|\hat{\mathbf{u}}\|_0.$$

Construct $\boldsymbol{\sigma}_h := \boldsymbol{\sigma}_{h,0} + \hat{\boldsymbol{\sigma}}$ and then we have:

$$(4.16) \quad (\mathbf{u}_h, \nabla \cdot \boldsymbol{\sigma}_h) = \underbrace{(\mathbf{u}_{h,0}, \nabla \cdot \boldsymbol{\sigma}_{h,0})}_{I_1} + \underbrace{(\hat{\mathbf{u}}, \nabla \cdot \boldsymbol{\sigma}_{h,0})}_{I_2} + \underbrace{(\mathbf{u}_{h,0}, \nabla \cdot \hat{\boldsymbol{\sigma}})}_{I_3} + \underbrace{(\hat{\mathbf{u}}, \nabla \cdot \hat{\boldsymbol{\sigma}})}_{I_4}.$$

For the first term, the B -compatibility of \mathcal{I}_h yields $I_1 = (\mathbf{u}_{h,0}, \mathbf{u}_{h,0}) = \|\mathbf{u}_{h,0}\|_0^2$. For the second term, applying Lemma 3.5 and the condition $\hat{\mathbf{u}} \in \mathcal{K}$ yields $I_2 = -(\boldsymbol{\sigma}_{h,0}, \mathcal{E}\hat{\mathbf{u}}) = 0$. Also, the third term vanishes due to orthogonality, and the fourth term simplifies to $I_4 = \|\hat{\mathbf{u}}\|_0^2$. Hence, we conclude that:

$$(4.17) \quad (\mathbf{u}_h, \nabla \cdot \boldsymbol{\sigma}_h) = \|\mathbf{u}_{h,0}\|_0^2 + \|\hat{\mathbf{u}}\|_0^2.$$

Next, we estimate $\|\mathbf{u}_h\|_0$ and $\|\boldsymbol{\sigma}_h\|_1$. For $\mathbf{u}_h = \mathbf{u}_{h,0} + \hat{\mathbf{u}}$, we have:

$$(4.18) \quad \|\mathbf{u}_h\|_0^2 = \|\mathbf{u}_{h,0} + \hat{\mathbf{u}}\|_0^2 = \|\mathbf{u}_{h,0}\|_0^2 + \|\hat{\mathbf{u}}\|_0^2.$$

And for $\boldsymbol{\sigma}_h = \boldsymbol{\sigma}_{h,0} + \hat{\boldsymbol{\sigma}}$, the H^1 stability of \mathcal{I}_h and Cauchy inequality give:

$$(4.19) \quad \|\boldsymbol{\sigma}_h\|_1 \leq \|\boldsymbol{\sigma}_{h,0}\|_1 + \|\hat{\boldsymbol{\sigma}}\|_1 \lesssim \|\boldsymbol{\sigma}_0\|_1 + \|\hat{\mathbf{u}}\|_0 \lesssim \|\mathbf{u}_{h,0}\|_0 + \|\hat{\mathbf{u}}\|_0 \lesssim \|\mathbf{u}_{h,0}\|_0.$$

Therefore, for $\mathbf{u}_h \in \mathbf{U}_h$, there exists $\boldsymbol{\sigma}_h \in \Sigma_h$ such that

$$(4.20) \quad \frac{|(\mathbf{u}_h, \nabla \cdot \boldsymbol{\sigma}_h)|}{\|\boldsymbol{\sigma}_h\|_1 \|\mathbf{u}_h\|_0} \gtrsim \frac{\|\mathbf{u}_h\|_0^2}{\|\mathbf{u}_h\|_0 \|\mathbf{u}_h\|_0} = 1,$$

which yields the discrete inf-sup condition (4.12). \square

4.2. Coercivity on the discrete kernel. To verify the coercivity on the discrete kernel in (U-1), we first state the constraint characterizing $\ker B_h$,

$$(4.21) \quad (\mathbf{v}_h, \nabla \cdot \boldsymbol{\sigma}_h) + (\nabla p_h, \mathbf{v}_h) + (\gamma_h, \nabla \cdot \mathbf{s}_h) = 0 \quad \forall (\mathbf{v}_h, \gamma_h) \in \mathbf{U}_h \times \Theta_h.$$

For any $(\boldsymbol{\sigma}_h, \mathbf{s}_h, p_h) \in \ker B_h$, this implies the following orthogonal condition:

$$(4.22) \quad (\mathbf{v}_h, \nabla \cdot \boldsymbol{\sigma}_h + \nabla p_h) = 0, \quad \forall \mathbf{v}_h \in \mathbf{U}_h.$$

Since $\ker B_h \not\subseteq \ker B$, coercivity does not directly follow from the continuous case. Specifically, for (4.22), $\nabla \cdot \boldsymbol{\sigma}_h \neq -\nabla p_h$ in general. Consequently, our first step is to verify the bound:

$$(4.23) \quad \|\nabla p_h\|_0 \lesssim \|\boldsymbol{\sigma}_h\|_1.$$

Establishing this estimate allows us to subsequently apply Korn's inequalities to complete the proof.

To facilitate the analysis, let $\Pi_h : L^2(\Omega; \mathbb{R}^d) \rightarrow \mathbf{U}_h$ denote the global L^2 projection defined by $(\mathbf{v}_h, \mathbf{u} - \Pi_h \mathbf{u}) = 0$ for all $\mathbf{v}_h \in \mathbf{U}_h$. The orthogonality condition (4.22) implies $\Pi_h \nabla p_h = -\Pi_h (\nabla \cdot \boldsymbol{\sigma}_h)$, then yielding

$$(4.24) \quad \|\Pi_h \nabla p_h\|_0 = \|\Pi_h (\nabla \cdot \boldsymbol{\sigma}_h)\|_0 \leq \|\nabla \cdot \boldsymbol{\sigma}_h\|_0 \leq \|\boldsymbol{\sigma}_h\|_1.$$

Furthermore, we observe that

$$(4.25) \quad \|\Pi_h \nabla p_h\|_0 = \sup_{\mathbf{v}_h \in \mathbf{U}_h} \frac{(\mathbf{v}_h, \Pi_h \nabla p_h)}{\|\mathbf{v}_h\|_0} = \sup_{\mathbf{v}_h \in \mathbf{U}_h} \frac{(\mathbf{v}_h, \nabla p_h)}{\|\mathbf{v}_h\|_0}.$$

Therefore, (4.23) follows from the condition below:

LEMMA 4.6. *For any $p_h \in P_h$, there holds*

$$(4.26) \quad \sup_{\mathbf{v}_h \in \mathbf{U}_h} \frac{(\mathbf{v}_h, \nabla p_h)}{\|\mathbf{v}_h\|_0} \gtrsim \|\nabla p_h\|_0.$$

Consequently, if the orthogonality condition (4.22) holds, then

$$(4.27) \quad \|\nabla p_h\|_0 \lesssim \|\boldsymbol{\sigma}_h\|_1.$$

Proof. (4.26) is the Bercovier-Pironneau type discrete inf-sup condition for the $\mathbb{P}_d\mathbb{P}_{d-1}$ Taylor-Hood pair (\mathbf{U}_h, P_h) . The case $d = 2$ was established in [2]; for $d = 3$, the result follows from the macroelement technique as given in [3], provided every tetrahedron contains at least one vertex in the domain interior. Then using (4.24)–(4.26), we obtain $\|\boldsymbol{\sigma}_h\|_1 \geq \sup_{\mathbf{v}_h \in \mathbf{U}_h} \frac{(\mathbf{v}_h, \nabla p_h)}{\|\mathbf{v}_h\|_0} \gtrsim \|\nabla p_h\|_0$ and complete the proof. \square

We are now ready to establish the coercivity on the discrete kernel from (4.27).

THEOREM 4.7. *For any $\boldsymbol{\mathcal{S}}_h \in \ker B_h$, the following coercivity condition holds:*

$$(4.28) \quad \mathcal{A}(\boldsymbol{\mathcal{S}}_h, \boldsymbol{\mathcal{S}}_h) \gtrsim \|\boldsymbol{\mathcal{S}}_h\|_{\mathbb{T}}^2 := \|\mathbf{s}_h\|_1^2 + \|\boldsymbol{\sigma}_h\|_1^2 + \|p_h\|_1^2.$$

Proof. It suffices to verify (U-1), which means for any $(\boldsymbol{\sigma}_h, \mathbf{s}_h, p_h) \in \ker B_h$,

$$(4.29) \quad \|\text{sym } \nabla \mathbf{s}_h\|_0^2 + \|\mathbf{s}_h\|_0^2 + \|\text{Stf } \nabla \boldsymbol{\sigma}_h\|_0^2 + \|\boldsymbol{\sigma}_h\|_0^2 \gtrsim \|\mathbf{s}_h\|_1^2 + \|\boldsymbol{\sigma}_h\|_1^2 + \|p_h\|_1^2.$$

From Korn's inequality of the second type and [18, Lemma 3.11], we have

$$(4.30) \quad \|\text{sym } \nabla \mathbf{s}_h\|_0^2 + \|\mathbf{s}_h\|_0^2 \gtrsim \|\mathbf{s}_h\|_1^2, \quad \|\text{Stf } \nabla \boldsymbol{\sigma}_h\|_0^2 + \|\boldsymbol{\sigma}_h\|_0^2 \gtrsim \|\boldsymbol{\sigma}_h\|_1^2.$$

Hence to prove (4.29), it remains to show $\|\boldsymbol{\sigma}_h\|_1 \gtrsim \|p_h\|_1$. Since $p_h \in \tilde{H}^1$, the proof is completed by invoking Poincaré's inequality and Lemma 4.6. \square

4.3. The *a priori* error estimate. We are now in a position to establish an *a priori* error estimate.

THEOREM 4.8. *The Galerkin formulation (3.3) for the linearized R13 system admits a unique solution $(\mathcal{S}_h, \mathcal{U}_h) = (\boldsymbol{\sigma}_h, \mathbf{s}_h, p_h, \mathbf{u}_h, \theta_h)$, which satisfies the quasi-optimal estimate:*

$$(4.31) \quad \|(\mathcal{S}_h, \mathcal{U}_h) - (\mathcal{S}, \mathcal{U})\|_{\mathbf{T} \times \mathbf{W}} \lesssim \inf_{(\mathcal{R}_h, \mathcal{V}_h) \in \mathbf{T}_h \times \mathbf{W}_h} \|(\mathcal{R}_h, \mathcal{V}_h) - (\mathcal{S}, \mathcal{U})\|_{\mathbf{T} \times \mathbf{W}}.$$

Furthermore, assume the exact solution $(\mathcal{S}, \mathcal{U}) = (\boldsymbol{\sigma}, \mathbf{s}, p, \mathbf{u}, \theta)$ satisfies

$$(4.32) \quad \boldsymbol{\sigma} \in H^{d+1}(\Omega; \mathbb{T}), \quad \mathbf{s} \in H^{d+1}(\Omega; \mathbb{R}^d), \quad p \in \tilde{H}^{d+1}(\Omega), \quad \mathbf{u} \in H^d(\Omega; \mathbb{R}^d), \quad \theta \in H^d(\Omega),$$

then the following *a priori* error estimate holds:

$$(4.33) \quad \begin{aligned} \|\boldsymbol{\sigma} - \boldsymbol{\sigma}_h\|_1 + \|\mathbf{s} - \mathbf{s}_h\|_1 + \|p - p_h\|_1 + \|\mathbf{u} - \mathbf{u}_h\|_0 + \|\theta - \theta_h\|_0 \\ \lesssim h^{d-1}|p|_d + h^d(|\boldsymbol{\sigma}|_{d+1} + |\mathbf{s}|_{d+1} + |\mathbf{u}|_d + |\theta|_d). \end{aligned}$$

Proof. The boundedness of the bilinear operators follows from the continuous formulation; see [18, Appendix A]. The coercivity on the discrete kernel and the discrete inf-sup conditions are established in Theorems 4.1, 4.5, and 4.7. Consequently, the standard Babuška-Brezzi theory implies the unisolvence of the Galerkin formulation (3.3) and the quasi-optimal error estimate (4.31). The final *a priori* error bound follows directly from standard interpolation estimates. \square

Regarding the L^2 norm error estimate, which is often of greater practical significance, we anticipate a gain of one order of convergence compared to the energy norm. Here we establish this result using a duality argument, under the assumption of *elliptic regularity* for the dual problem.

COROLLARY 4.9. *Let $\mathbf{e}_{\mathcal{S}} = \mathcal{S} - \mathcal{S}_h$ and $\mathbf{e}_{\mathcal{U}} = \mathcal{U} - \mathcal{U}_h$. Assume that the dual problem (4.36)-(4.37) (defined in the proof below) admits the elliptic regularity property*

$$(4.34) \quad \|\mathbf{T}\|_2 + \|\mathbf{W}\|_1 \lesssim \|\mathbf{e}_{\mathcal{S}}\|_0.$$

Then, the following estimate holds:

$$(4.35) \quad \|\boldsymbol{\sigma} - \boldsymbol{\sigma}_h\|_0 + \|\mathbf{s} - \mathbf{s}_h\|_0 + \|p - p_h\|_0 \lesssim h^d|p|_d + h^{d+1}(|\boldsymbol{\sigma}|_{d+1} + |\mathbf{s}|_{d+1} + |\mathbf{u}|_d + |\theta|_d).$$

Proof. Consider the dual problem: seek $(\mathbf{T}, \mathbf{W}) \in \mathbf{T} \times \mathbf{W}$ such that

$$(4.36) \quad \mathcal{A}(\mathcal{R}, \mathbf{T}) + \mathcal{B}(\mathcal{R}, \mathbf{W}) = (\mathbf{e}_{\mathcal{S}}, \mathcal{R}) \quad \forall \mathcal{R} \in \mathbf{T},$$

$$(4.37) \quad \mathcal{B}(\mathbf{T}, \mathcal{V}) = 0 \quad \forall \mathcal{V} \in \mathbf{W}.$$

By testing (4.36) and (4.37) with $\mathcal{R} = \mathbf{e}_{\mathcal{S}}$ and $\mathcal{V} = \mathbf{e}_{\mathcal{U}}$, and employing the Galerkin orthogonality, we obtain

$$(4.38) \quad \begin{aligned} \|\mathbf{e}_{\mathcal{S}}\|_0^2 &= \mathcal{A}(\mathbf{e}_{\mathcal{S}}, \mathbf{T} - \mathbf{T}_h) - \mathcal{B}(\mathbf{T}_h, \mathbf{e}_{\mathcal{U}}) + \mathcal{B}(\mathbf{e}_{\mathcal{S}}, \mathbf{W} - \mathbf{W}_h) \\ &= \mathcal{A}(\mathbf{e}_{\mathcal{S}}, \mathbf{T} - \mathbf{T}_h) + \mathcal{B}(\mathbf{T} - \mathbf{T}_h, \mathbf{e}_{\mathcal{U}}) + \mathcal{B}(\mathbf{e}_{\mathcal{S}}, \mathbf{W} - \mathbf{W}_h) \\ &\lesssim (\|\mathbf{e}_{\mathcal{S}}\|_{\mathbf{T}} + \|\mathbf{e}_{\mathcal{U}}\|_{\mathbf{W}}) \cdot h (\|\mathbf{T}\|_2 + \|\mathbf{W}\|_1). \end{aligned}$$

Applying the regularity assumption (4.34) allows us to cancel one factor of $\|\mathbf{e}_{\mathcal{S}}\|_0$, yielding $\|\mathbf{e}_{\mathcal{S}}\|_0 \lesssim h (\|\mathbf{e}_{\mathcal{S}}\|_{\mathbf{T}} + \|\mathbf{e}_{\mathcal{U}}\|_{\mathbf{W}})$. Combining this result with the energy norm estimates in Theorem 4.8 gives the desired bound (4.35). \square

Remark 4.10. The global convergence rates in Theorem 4.8 and Corollary 4.9 are limited by the pressure error. Such behavior reflects a necessary trade-off between conformity and stability under a specific choice of H^1 pressure and L^2 velocity spaces in the current weak form.

5. Numerical experiments. This section presents numerical results for the MFEM (3.3) with finite element spaces in (3.1). We demonstrate the stability and convergence of the method, with $\tilde{\chi} = 1$ for all test cases. The scheme is implemented using the MATLAB package `ifem` [10].

5.1. Homogeneous flow around a cylinder. We first test Couette-Fourier flows within an annular domain $\Omega \subset \mathbb{R}^2$ defined by

$$(5.1) \quad \Omega := \{\mathbf{x} = (x, y)^T : R_1 \leq \|\mathbf{x}\|_2 \leq R_2\},$$

with $R_1 = 0.5$ and $R_2 = 2$. Simulations are performed on body-fitted triangular meshes generated via the `distmesh2d` function in `ifem`.

Example 5.1. This case simulates Couette-Fourier flow driven by two uniformly rotating cylinders held at constant temperatures. The parameters are defined as:

$$(5.2) \quad \begin{aligned} u_t^W|_{\|\mathbf{x}\|=R_1} &= u_t^W|_{\|\mathbf{x}\|=R_2} = 1, & \theta^W|_{\|\mathbf{x}\|=R_1} &= \theta^W|_{\|\mathbf{x}\|=R_2} = 1, \\ \text{Kn} &= 0.05, 0.1, 0.2, 0.4, & h &= 0.2, 0.1, 0.05, 0.025, 0.0125, \end{aligned} \quad \text{respectively.}$$

We define the *absolute L^2 error* as

$$(5.3) \quad e_f := \|f_{\text{exact}} - f_h\|_0.$$

The analytical solution is derived from [26, Appendix A]. Figure 1 plots the errors against the mesh size h . The results confirm the second-order convergence of the proposed scheme across various Knudsen numbers.

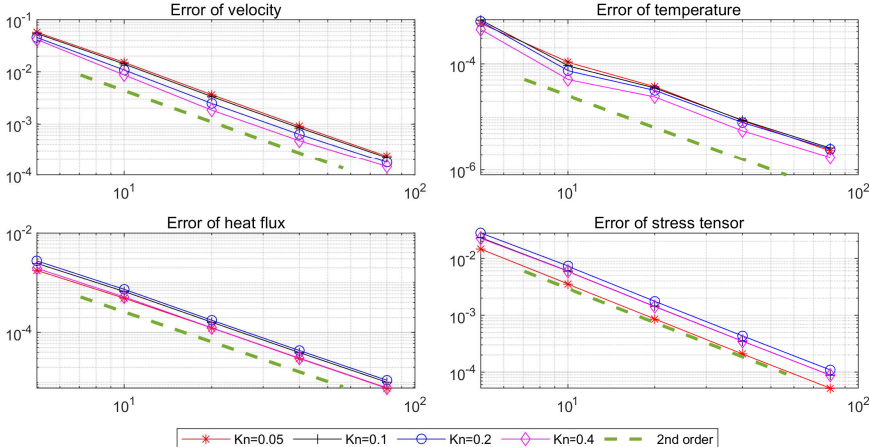


FIG. 1. The absolute L^2 error for each unknown in the R13 system.

Example 5.2. Next, we investigate the Couette-Fourier flow where the outer wall temperature differs from the inner wall. The parameters are:

$$(5.4) \quad \begin{aligned} u_t^W|_{\|\mathbf{x}\|=R_1} &= u_t^W|_{\|\mathbf{x}\|=R_2} = 1, & \theta^W|_{\|\mathbf{x}\|=R_1} &= 1, & \theta^W|_{\|\mathbf{x}\|=R_2} &= 2, \\ \text{Kn} &= 0.1, & h &= 0.1. \end{aligned}$$

We compare the proposed scheme with the unenriched $\mathbb{P}_2\text{-}\mathbb{P}_2\text{-}\mathbb{P}_1\text{-}\mathbb{P}_2\text{-}\mathbb{P}_1$ element. Since the unenriched formulation yields a singular linear system, we pick the solution with the minimum norm. The resulting θ , u_x and u_y profiles are presented in Figure 2. As detailed in Figure 2b, the velocity field exhibits spurious oscillations. This confirms the necessity of stabilizing Σ_h via enrichment with bubble functions, or the penalty terms proposed in [38].

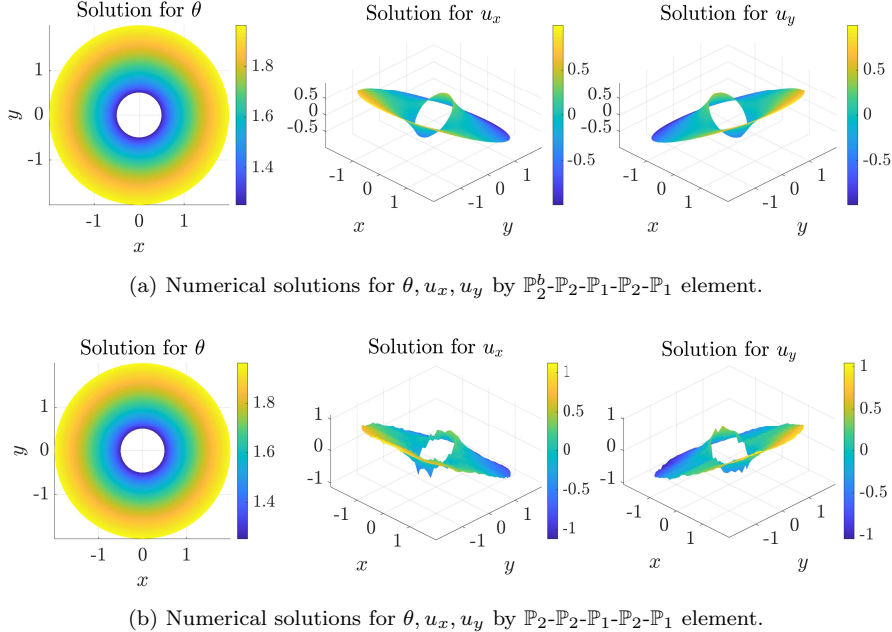


FIG. 2. Temperature and velocity distributions for Couette-Fourier flow around a cylinder.

5.2. Channel flow within a square cavity. We consider the channel flow within a square cavity. The problem domain is the unit square $\Omega := (0, 1)^2$ using uniform triangulations. The boundary $\partial\Omega$ is partitioned into the bottom wall Γ_1 and the remainder Γ_2 , with $\Gamma_1 := \{(x, y) : y = 0, x \in (0, 1)\}$, $\Gamma_2 := \partial\Omega \setminus \Gamma_1$. Note that singularities will arise in the solution at the lower corners.

Example 5.3. We simulate Fourier flow with fixed walls ($u_t^W = 0$). The bottom boundary Γ_1 is heated, while Γ_2 is held at a lower temperature. We vary the Knudsen number Kn to analyze heat conduction regimes using the following parameters:

$$(5.5) \quad \begin{aligned} u_t^W|_{\Gamma_1} &= u_t^W|_{\Gamma_2} = 0, & \theta^W|_{\Gamma_1} &= 1, & \theta^W|_{\Gamma_2} &= 0, \\ \text{Kn} &= 0.01, 0.05, 0.2, \text{ respectively}, & h &= 0.02. \end{aligned}$$

Figure 3 displays the temperature distributions for various values of Kn . As expected physically, heat transfer is more efficient in the continuum regime (lower Kn), resulting in deeper thermal propagation from Γ_1 . The proposed scheme accurately captures this behavior, demonstrating its robustness in resolving the physics of the small Kn limit.

5.3. Thermally-induced edge flow.

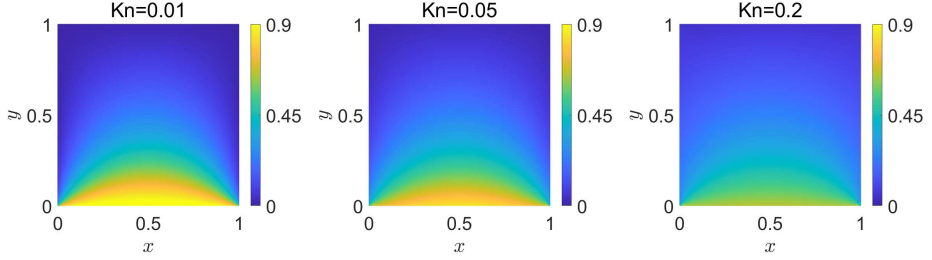


FIG. 3. Temperature distributions for Fourier flow in a square cavity.

Example 5.4. Finally, we investigate the thermally-induced edge flow, a benchmark problem from [38, Section 6.3]. The computational domain Ω is a square with an inner square obstacle defined by $\Omega := (0, 8)^2 \setminus [1, 3]^2$. Both the inner and outer boundaries are stationary no-slip walls. A temperature difference is imposed such that the outer boundary is maintained at a lower temperature than the inner boundary, and we set $\text{Kn} = 0.001$. This choice falls within the near-continuum regime and is used to validate the asymptotic preservation properties of kinetic schemes [35, 36]. The parameters are summarized as:

$$(5.6) \quad u_t^W|_{\text{inner}} = u_t^W|_{\text{outer}} = 0, \quad \theta^W|_{\text{inner}} = 0, \quad \theta^W|_{\text{outer}} = 1, \quad \text{Kn} = 0.001.$$

First, we present the shear stress and thermal fields computed with a mesh size of $h = 0.01$ in Figure 4. The left panel displays a stable shear stress field σ_{12} , and the right panel depicts temperature θ contours and heat flux \mathbf{s} streamlines consistent with Fourier's law.

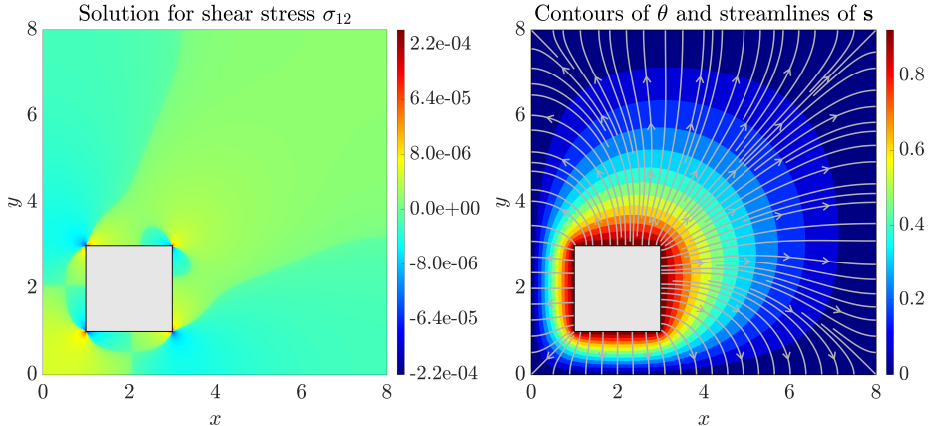
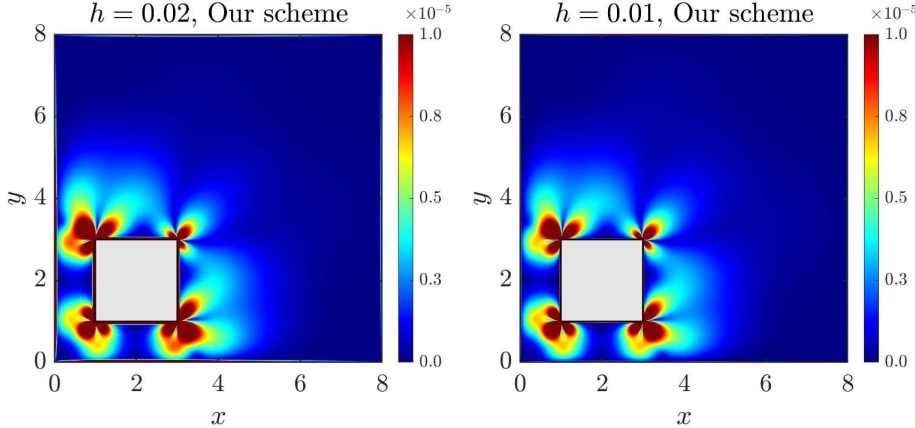


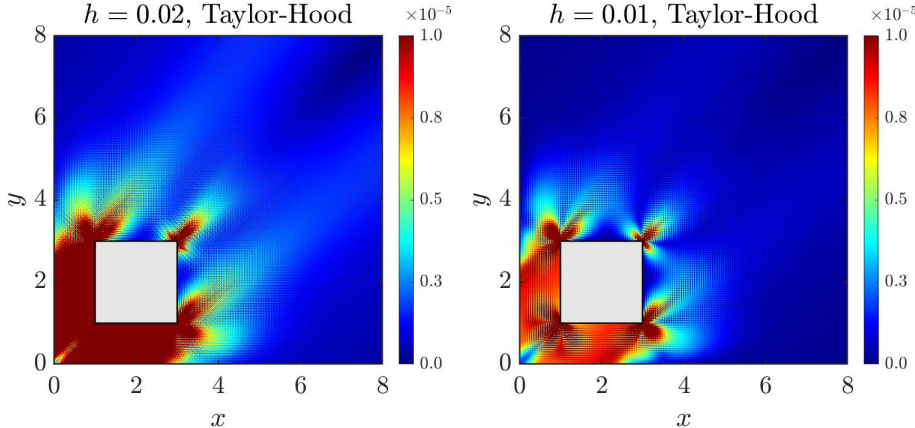
FIG. 4. Shear stress and heat distributions for the thermally-induced edge flow.

Next, we assess numerical stability by comparing our proposed scheme against the standard Taylor-Hood element ($\mathbb{P}_2\text{-}\mathbb{P}_1\text{-}\mathbb{P}_1\text{-}\mathbb{P}_2\text{-}\mathbb{P}_1$) on uniform meshes with $h = 0.02$ and $h = 0.01$. As illustrated in Figure 5, the Taylor-Hood element exhibits significant instability, characterized by spurious checkerboard modes in the velocity magnitude. In contrast, the proposed scheme remains robust and stable under identical conditions,

accurately capturing the rarefaction effects inherent in the edge flow.



(a) Velocity magnitudes computed by $\mathbb{P}_2^b\text{-}\mathbb{P}_2\text{-}\mathbb{P}_1\text{-}\mathbb{P}_2\text{-}\mathbb{P}_1$ element.



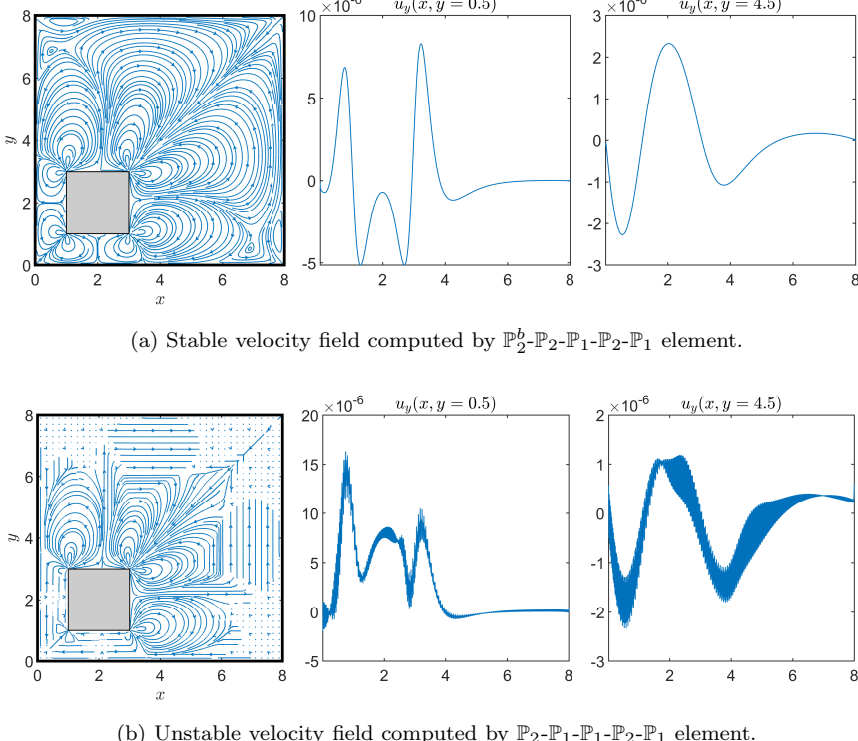
(b) Velocity magnitudes computed by $\mathbb{P}_2\text{-}\mathbb{P}_1\text{-}\mathbb{P}_1\text{-}\mathbb{P}_2\text{-}\mathbb{P}_1$ element.

FIG. 5. Velocity magnitude distributions for the thermally-induced edge flow.

Finally, we take a closer look at the solution on the fine mesh with $h = 0.01$. Figure 6 displays the velocity streamlines and profiles of vertical velocity u_y at $y = 0.5$ and $y = 4.5$. While the standard Taylor-Hood element produces pronounced oscillations, our scheme successfully resolves the flow structure, demonstrating its effectiveness and accuracy in this challenging regime.

6. Conclusions. In this paper, we have proposed and analyzed a novel conforming MFEM for the linear R13 equations. By enriching the tensor element space with specific bubble functions, we successfully establish a stable, convergent, and penalty-free scheme with rigorous theoretical analysis.

The proposed framework offers significant advantages for further research. First, our scheme can be extended to R13 systems with inflow or outflow boundary conditions. Second, for time-dependent R13 systems, as discussed in [19], designing stable schemes using CIP methods can be impractical due to parameter tuning; our penalty-free approach provides a more natural and robust foundation for such extensions.

FIG. 6. Velocity streamlines and u_y profiles for the thermally-induced edge flow.

Third, the inherent stability of our scheme makes it highly suitable for simulating complex rarefied gas phenomena.

Given that the enriched space increases the number of degrees of freedom, future work will focus on developing efficient preconditioners for fast solvers and reduced-basis methods to mitigate computational costs. Additionally, extending this rigorous MFEM framework to time-dependent cases or to other R13 systems for general gas molecules, as described in [8], is a promising direction for future investigation.

Appendix A. Korn-type inequalities.

In this section, we review \mathbb{C} -ellipticity for first-order linear homogeneous differential operators and prove Theorem A.4.

DEFINITION A.1. Let $V = \mathbb{R}^d$ and $W = \mathbb{R}^{d'}$. A first-order linear homogeneous operator with constant coefficients $\mathbb{A} := \sum_{j=1}^d \mathbb{A}_j \partial_j$, where $\mathbb{A}_j \in L(V, W)$, is called \mathbb{C} -elliptic, if the corresponding symbol map $\mathbb{A}[\xi] : \mathbb{C}^d \rightarrow \mathbb{C}^{d'}$, $\mathbb{A}[\xi](v) := \sum_{j=1}^d \xi_j \mathbb{A}_j v$ ($\xi \in \mathbb{C}^d$) has no common non-trivial complex zero. That is,

$$(A.1) \quad \forall \xi \in \mathbb{C}^d, \quad \mathbb{A}[\xi](v) = 0 \quad \implies \quad v = 0.$$

Then we have the following ellipticity condition for the operator $\text{stf } \nabla$.

THEOREM A.2. The operator $\text{stf } \nabla$ acting on vector fields is \mathbb{C} -elliptic if and only if the dimension $d \geq 3$.

Proof. To establish the \mathbb{C} -ellipticity of $P := \text{stf } \nabla$, it suffices to show that its symbol is injective for any $\xi \in \mathbb{C}^d \setminus \{0\}$. As noted in [18, Remark 3.4], the symbol is

given by $P[\xi](v) = \text{stf}(v \otimes \xi)$; therefore, injectivity is equivalent to the condition:

$$(A.2) \quad \text{stf}(v \otimes \xi) = 0 \implies v = 0.$$

Let $v = (v_i)$ and $\xi = (\xi_j)$. The condition (A.2) implies:

$$(A.3) \quad v_i \xi_i = v_j \xi_j, \quad v_i \xi_j = -v_j \xi_i, \quad \forall i \neq j.$$

If $d = 2$, the vectors $v = (i, 1)^T$ and $\xi = (i, -1)^T$ serve as a counterexample for (A.3). If $d \geq 3$, consider two cases. First, suppose ξ contains zero components. Up to permutation, let $\xi_1 = \xi_2 = \dots = \xi_j = 0$ and $\xi_l \neq 0$ for all $l > j$. Since $v_i \xi_i \equiv v_l \xi_l$ implies $v_l \xi_l = 0$ (as we can pick an index from the zero components), and $\xi_l \neq 0$, it follows that $v_l = 0$ for all $l > j$. For the indices $k \leq j$, we have $v_k \xi_{j+1} = -v_{j+1} \xi_k$. Since $v_{j+1} = 0$ and $\xi_{j+1} \neq 0$, this implies $v_k = 0$ and thus $v = 0$. Second, assume all components of ξ are non-zero. Then the latter equation in (A.3) combined with the first implies that for any $i \neq j$, $v_i^2 \xi_j = -v_j \xi_i v_i = -v_i \xi_i v_j = -v_j \xi_j v_j$, which simplifies to $v_i^2 + v_j^2 = 0$ and leads to $v = 0$. \square

The following theorem shows the relationship between \mathbb{C} -ellipticity and Korn-type inequalities.

THEOREM A.3. *Let $\Omega \subset \mathbb{R}^3$ be a bounded Lipschitz domain, \mathbb{A} is a first-order linear homogeneous operator with constant coefficients, then the following inequality holds if and only if \mathbb{A} is a \mathbb{C} -elliptic operator:*

$$(A.4) \quad \|\mathbf{u}\|_s \lesssim \|\mathbf{u}\|_t + \|\mathbb{A}\mathbf{u}\|_{s-1}, \quad \text{for } t < s.$$

Proof. See [30, Corollary 7.3]. \square

Finally, we present the proof for the generalized Korn's inequality of a negative norm.

THEOREM A.4. *For a bounded Lipschitz domain $\Omega \subset \mathbb{R}^3$ and $\mathbf{v} \in L^2(\Omega; \mathbb{R}^3)$, the generalized Korn's inequality of negative norm holds:*

$$(A.5) \quad \|\mathbf{v}\|_0 \lesssim \|\text{stf } \nabla \mathbf{v}\|_{-1} + \|\mathbf{v}\|_{-1}.$$

Proof. The operator $P := \text{stf } \nabla$ is a first-order, linear homogeneous differential operator. As established in Theorem A.2, P is \mathbb{C} -elliptic for $d \geq 3$. Consequently, we can directly apply Korn-type inequality in Theorem A.3. This corollary provides the following a priori estimate for $u \in H^s(\Omega)$:

$$(A.6) \quad \|u\|_s \lesssim \|Pu\|_{s-1} + \|u\|_t,$$

where $t < s$ is an arbitrary lower-order index. Setting $s = 0$ and $t = -1$ yields the desired result. \square

Acknowledgments. The authors would like to thank Ziwen Gu from Shanghai University of Finance and Economics for his valuable suggestions regarding conforming tensor-valued elements.

REFERENCES

[1] Q. AN, X. HUANG, AND C. ZHANG, *A decoupled finite element method for the triharmonic equation*, Applied Mathematics Letters, 147 (2024), p. 108843, <https://doi.org/10.1016/j.aml.2023.108843>.

- [2] M. BERCOVIER AND O. PIRONNEAU, *Error estimates for finite element method solution of the Stokes problem in the primitive variables*, Numerische Mathematik, 33 (1979), pp. 211–224, <https://doi.org/10.1007/BF01399555>.
- [3] D. BOFFI, *Three-dimensional finite element methods for the Stokes problem*, SIAM Journal on Numerical Analysis, 34 (1997), pp. 664–670, <https://doi.org/10.1137/S0036142994270193>.
- [4] F. BOYER AND P. FABRIE, *Mathematical tools for the study of the incompressible Navier-Stokes equations and related models*, vol. 183 of Applied Mathematical Sciences, Springer, New York, 2013, <https://doi.org/10.1007/978-1-4614-5975-0>.
- [5] S. C. BRENNER AND L. R. SCOTT, *The mathematical theory of finite element methods*, Springer, New York, 2008, <https://doi.org/10.1007/978-0-387-75934-0>.
- [6] F. BREZZI, *On the existence, uniqueness and approximation of saddle-point problems arising from Lagrangian multipliers*, RAIRO. Analyse Numérique, 8 (1974), pp. 129–151, <https://doi.org/10.1051/m2an/197408R201291>.
- [7] F. BREZZI AND R. S. FALK, *Stability of higher-order Hood–Taylor methods*, SIAM Journal on Numerical Analysis, 28 (1991), pp. 581–590, <https://doi.org/10.1137/0728032>.
- [8] Z. CAI, M. TORRILHON, AND S. YANG, *Linear regularized 13-moment equations with Onsager boundary conditions for general gas molecules*, SIAM Journal on Applied Mathematics, 84 (2024), pp. 215–245, <https://doi.org/10.1137/23M1556472>.
- [9] Z. CAI AND Y. WANG, *Regularized 13-moment equations for inverse power law models*, Journal of Fluid Mechanics, 894 (2020), p. A12, <https://doi.org/10.1017/jfm.2020.251>.
- [10] L. CHEN, *iFEM: an integrated finite element methods package in MATLAB*, tech. report, University of California at Irvine, 2009, <https://github.com/lyc102/ifem>.
- [11] P. G. CIARLET, *On Korn’s inequality*, Chinese Annals of Mathematics, Series B, 31 (2010), pp. 607–618, <https://doi.org/10.1007/s11401-010-0606-3>.
- [12] R. CLAYDON, A. SHRESTHA, A. S. R. J. E. SPRITTLES, AND D. A. LOCKERBY, *Fundamental solutions to the regularised 13-moment equations: efficient computation of three-dimensional kinetic effects*, Journal of Fluid Mechanics, 833 (2017), p. R4, <https://doi.org/10.1017/jfm.2017.763>.
- [13] T. C. DE FRAJA, A. S. RANA, R. ENRIGHT, L. J. COOPER, D. A. LOCKERBY, AND J. E. SPRITTLES, *Efficient moment method for modeling nanoporous evaporation*, Physical Review Fluids, 7 (2022), p. 024201, <https://doi.org/10.1103/PhysRevFluids.7.024201>.
- [14] G. DUVAUT AND J. L. LIONS, *Inequalities in Mechanics and Physics*, Springer Berlin, Heidelberg, 2012, <https://doi.org/10.1007/978-3-642-66165-5>.
- [15] H. GRAD, *On the kinetic theory of rarefied gases*, Communications on Pure and Applied Mathematics, 2 (1949), pp. 331–407, <https://doi.org/https://doi.org/10.1002/cpa.3160020403>.
- [16] HIMANSHI, L. THEISEN, A. S. RANA, M. TORRILHON, AND V. K. GUPTA, *A generalized fundamental solution technique for the regularized 13-moment system in rarefied gas flows*, Journal of Computational Physics, 549 (2026), p. 114591, <https://doi.org/10.1016/j.jcp.2025.114591>.
- [17] C. D. LEVERMORE, *Moment closure hierarchies for kinetic theories*, Journal of Statistical Physics, 83 (1996), pp. 1021–1065, <https://doi.org/10.1007/BF02179552>.
- [18] P. LEWINTAN, L. THEISEN, AND M. TORRILHON, *Well-posedness of the R13 equations using tensor-valued Korn inequalities*, 2025, <https://arxiv.org/abs/2501.14108>.
- [19] B. LIN, H. WANG, S. YANG, AND Z. CAI, *Time-dependent regularised 13-moment equations with Onsager boundary conditions in the linear regime*, Journal of Fluid Mechanics, 1009 (2025), p. A60, <https://doi.org/10.1017/jfm.2025.215>.
- [20] J. McDONALD AND M. TORRILHON, *Affordable robust moment closures for CFD based on the maximum-entropy hierarchy*, Journal of Computational Physics, 251 (2013), pp. 500–523, <https://doi.org/10.1016/j.jcp.2013.05.046>.
- [21] K. MÜLLER, *Computing rarefied external flows using extended fluid dynamics*, master’s thesis, Swiss Federal Institute of Technology Zurich, 2010.
- [22] R. S. MYONG, *Thermodynamically consistent hydrodynamic computational models for high-Knudsen-number gas flows*, Physics of Fluids, 11 (1999), pp. 2788–2802, <https://doi.org/10.1063/1.870137>.
- [23] A. S. RANA, A. MOHAMMADZADEH, AND H. STRUCHTRUP, *A numerical study of the heat transfer through a rarefied gas confined in a microcavity*, Continuum Mechanics and Thermodynamics, 27 (2015), pp. 433–446, <https://doi.org/10.1007/s00161-014-0371-8>.
- [24] A. S. RANA AND H. STRUCHTRUP, *Thermodynamically admissible boundary conditions for the regularized 13 moment equations*, Physics of Fluids, 28 (2016), p. 027105, <https://doi.org/10.1063/1.4941293>.
- [25] A. S. RANA, M. TORRILHON, AND H. STRUCHTRUP, *A robust numerical method for the R13 equations of rarefied gas dynamics: Application to lid driven cavity*, Journal of Computa-

tional Physics, 236 (2013), pp. 169–186, <https://doi.org/10.1016/j.jcp.2012.11.023>.

[26] A. K. SARAVANAKUMAR, *Investigation of the CIP stabilization parameters and extension of the FenicsR13 solver*, bachelor's thesis, Birla Institute of Technology and Science, Pilani, 2020.

[27] N. SARNA AND M. TORRILHON, *On stable wall boundary conditions for the Hermite discretization of the linearised Boltzmann equation*, Journal of Statistical Physics, 170 (2018), pp. 101–126, <https://doi.org/10.1007/s10955-017-1910-z>.

[28] O. D. SCHIRRA, *New Korn-type inequalities and regularity of solutions to linear elliptic systems and anisotropic variational problems involving the trace-free part of the symmetric gradient*, Calculus of Variations and Partial Differential Equations, 43 (2012), pp. 147–172, <https://doi.org/10.1007/s00526-011-0406-y>.

[29] L. R. SCOTT AND S. ZHANG, *Finite element interpolation of nonsmooth functions satisfying boundary conditions*, Mathematics of Computation, 54 (1990), pp. 483–493, <https://doi.org/10.1090/S0025-5718-1990-1011446-7>.

[30] K. SMITH, *Formulas to represent functions by their derivatives*, Mathematische Annalen, 188 (1970), pp. 53–77, <https://doi.org/10.1007/BF01435415>.

[31] R. STENBERG, *On some three-dimensional finite elements for incompressible media*, Computer Methods in Applied Mechanics and Engineering, 63 (1987), pp. 261–269, [https://doi.org/10.1016/0045-7825\(87\)90072-7](https://doi.org/10.1016/0045-7825(87)90072-7).

[32] H. STRUCHTRUP, *Macroscopic Transport Equations for Rarefied Gas Flows: Approximation Methods in Kinetic Theory*, vol. 1 of Interaction of Mechanics and Mathematics, Springer Berlin, Heidelberg, 2005, <https://doi.org/10.1007/3-540-32386-4>.

[33] H. STRUCHTRUP AND M. TORRILHON, *Regularization of Grad's 13 moment equations: Derivation and linear analysis*, Physics of Fluids, 15 (2003), pp. 2668–2680, <https://doi.org/10.1063/1.1597472>.

[34] H. STRUCHTRUP AND H. C. ÖTTINGER, *Thermodynamically admissible 13-moment equations*, Physics of Fluids, 34 (2022), p. 017105, <https://doi.org/10.1063/5.0078780>.

[35] W. SU, P. WANG, Y. ZHANG, AND L. WU, *Implicit discontinuous Galerkin method for the Boltzmann equation*, Journal of Scientific Computing, 82 (2020), p. 39, <https://doi.org/10.1007/s10915-020-01139-7>.

[36] W. SU, L. ZHU, AND L. WU, *Fast convergence and asymptotic preserving of the general synthetic iterative scheme*, SIAM Journal on Scientific Computing, 42 (2020), pp. B1517–B1540, <https://doi.org/10.1137/20M132691X>.

[37] P. TAHERI AND M. BAHRAMI, *Macroscopic description of nonequilibrium effects in thermal transpiration flows in annular microchannels*, Physical Review E, 86 (2012), p. 036311, <https://doi.org/10.1103/PhysRevE.86.036311>.

[38] L. THEISEN AND M. TORRILHON, *fenicsR13: a tensorial mixed finite element solver for the linear R13 equations using the FEniCS computing platform*, ACM Transactions on Mathematical Software, 47 (2021), pp. Art. 17, 29, <https://doi.org/10.1145/3442378>.

[39] L. THEISEN AND M. TORRILHON, *fenicsR13: a tensorial mixed finite element solver for the linear R13 equations using the FEniCS computing platform*, 2025, <https://doi.org/10.5281/zenodo.14938147>. Version 1.5.

[40] M. Y. TIMOKHIN, H. STRUCHTRUP, A. A. KOKHANCHIK, AND Y. A. BONDAR, *Different variants of R13 moment equations applied to the shock-wave structure*, Physics of Fluids, 29 (2017), p. 037105, <https://doi.org/10.1063/1.4977978>.

[41] M. TORRILHON AND H. STRUCHTRUP, *Boundary conditions for regularized 13-moment-equations for micro-channel-flows*, Journal of Computational Physics, 227 (2008), pp. 1982–2011, <https://doi.org/10.1016/j.jcp.2007.10.006>.

[42] A. WESTERKAMP AND M. TORRILHON, *Finite element discretizations for extended gas dynamics*, master's thesis, RWTH Aachen University, 2012.

[43] A. WESTERKAMP AND M. TORRILHON, *Curvature-induced instability of a Stokes-like problem with non-standard boundary conditions*, Applied Numerical Mathematics, 121 (2017), pp. 96–114, <https://doi.org/10.1016/j.apnum.2017.06.012>.

[44] A. WESTERKAMP AND M. TORRILHON, *Finite element methods for the linear regularized 13-moment equations describing slow rarefied gas flows*, Journal of Computational Physics, 389 (2019), pp. 1–21, <https://doi.org/10.1016/j.jcp.2019.03.022>.

**SUPPLEMENTARY MATERIALS: STABILITY AND
CONVERGENCE OF MIXED FINITE ELEMENTS FOR LINEAR
REGULARIZED 13-MOMENT EQUATIONS ***

SHUANG HU[†], HUITENG LI[‡], AND ZHENNING CAI[§]

SM1. Interpolation operator. In this section, we prove Lemma 3.3 for $d = 2$. First, we derive the dual basis for $\Sigma_{h,0}$ with corresponding DoFs (3.4). For each element $K \subset \Omega$, we mark DoFs on element K in Figure SM1a and derive its dual basis.

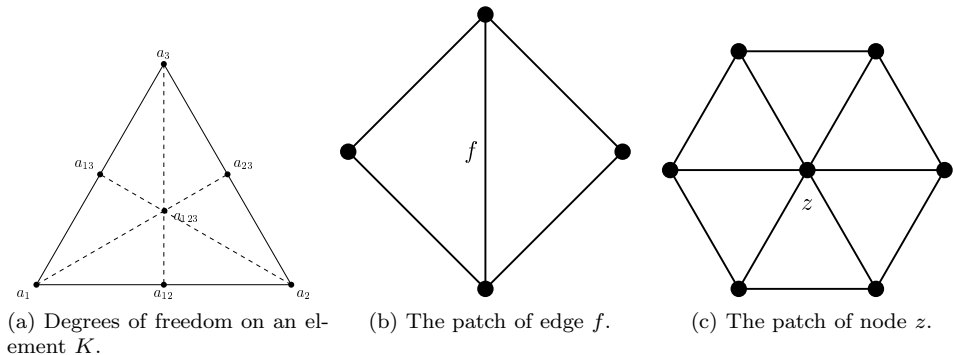


FIG. SM1. *Figures related to DoFs and dual basis.*

Since $\tau_h \in \Sigma_h$ should be a symmetric 2×2 tensor, the dual basis of Σ_h shows the following form:

$$(SM1.1) \quad \left\{ \begin{bmatrix} u & 0 \\ 0 & 0 \end{bmatrix}, \quad \begin{bmatrix} 0 & u \\ u & 0 \end{bmatrix}, \quad \begin{bmatrix} 0 & 0 \\ 0 & u \end{bmatrix} \right\},$$

and the dual basis functions on each DoF:

- On nodal points a_i , the basis functions:

$$(SM1.2) \quad u_i = \lambda_i(3\lambda_i - 2) + \lambda_1\lambda_2\lambda_3(24 - 42\lambda_i).$$

- On edge a_{ij} , the basis functions:

$$(SM1.3) \quad u_{ij} = \frac{6}{|a_{ij}|}(\lambda_i\lambda_j + \lambda_1\lambda_2\lambda_3(21\lambda_k - 12)),$$

where $k \neq i, j$.

* Shuang Hu and Huiteng Li are co-first authors with equal contributions.

Funding: The work of Zhenning Cai was supported by the Academic Research Fund of the Ministry of Education of Singapore under Grant No. A-8002392-00-00.

[†] Zhejiang University, 866 Yuhangtang Road, Hangzhou, Zhejiang Province, 310058 China (hs-mathnra@gmail.com).

[‡] King Abdullah University of Science and Technology (KAUST), Thuwal, 23955 Saudi Arabia (huiteng.li@kaust.edu.sa).

[§] Corresponding author. Department of Mathematics, National University of Singapore, Level 4, Block S17, 10 Lower Kent Ridge Road, Singapore 119076 (matcz@nus.edu.sg).

- On the element K (marked as a_{123}), the basis function (e.g., the first one):

$$(SM1.4) \quad u_{123,1} = \frac{1}{|K|} \lambda_1 \lambda_2 \lambda_3 (900\lambda_1 - 360\lambda_2 - 360\lambda_3),$$

where $|K|$ denotes the area of element K .

From (SM1.2), (SM1.3) and (SM1.4), we can construct the global “hat-basis” for Σ_h . The **patch** of a node z or an edge f , marked as \mathcal{T}_z or \mathcal{T}_f , consists of all the elements K which share common node z (or edge f), see Figure SM1b, Figure SM1c. Then the entry of the global basis functions of node z , edge f and element K can write as

$$(SM1.5) \quad \phi_z := \sum_{K \in \mathcal{T}_z} \chi_K u_{K,z}, \quad \tau_f := \sum_{K \in \mathcal{T}_f} \chi_K u_{K,f}, \quad \varphi_{K,i} := \chi_K u_{K,i} \quad (1 \leq i \leq 3),$$

respectively. Now, we show the proof for Lemma 3.3.

Proof for Lemma 3.3. First, we show the operator \mathcal{I}_h is a projection onto Σ_h . It suffices to show that \mathcal{I}_h is the identity on Σ_h . By the definition, if $\tau \in \Sigma_h$, we have $Q_K \tau = \tau$ always holds on K . Then (3.5) yields:

$$(SM1.6) \quad \begin{aligned} I_h \tau(\delta) &= \tau(\delta), \\ (\mathcal{I}_h \tau, \mathbf{q})_f &= (\tau, \mathbf{q})_f \quad \forall \mathbf{q} \in \mathbb{P}_0, \\ (\mathcal{I}_h \tau, \mathbf{q})_K &= (\tau, \mathbf{q})_K \quad \forall \mathbf{q} \in \epsilon(\mathbb{P}_1(K; \mathbb{R}^2)), \end{aligned}$$

since the DoFs in (SM1.6) are identical with (3.4), it means that $\mathcal{I}_h \tau = \tau$ on Σ_h and thus $\mathcal{I}_h^2 = \mathcal{I}_h$, i.e., \mathcal{I}_h is a projection.

Next, we will show the second result: L^2 -estimation. We consider the estimation on the element $K \subset \Omega$. \tilde{K} denotes the union of all mesh elements that intersect K , which is called the **first-order patch** of K .

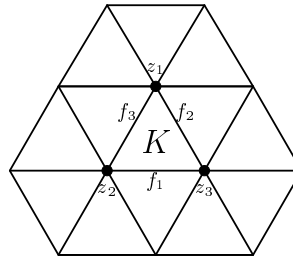


FIG. SM2. The first-order patch \tilde{K} of element K .

By Poincaré's inequality, we can choose a constant $C_{\tilde{K}} := \frac{1}{|\tilde{K}|} \int_{\tilde{K}} \tau$ such that

$$(SM1.7) \quad \|\tau - C_{\tilde{K}}\|_{0,\tilde{K}} \lesssim h |\tau|_{1,\tilde{K}}.$$

Mark $w := \tau - C_{\tilde{K}}$, since $I_h C_{\tilde{K}} = C_{\tilde{K}}$, we have:

$$(SM1.8) \quad \|\tau - I_h \tau\|_{0,K} \leq \|\tau - C_{\tilde{K}}\|_{0,K} + \|\mathcal{I}_h(\tau - C_{\tilde{K}})\|_{0,K} = \|w\|_{0,K} + \|\mathcal{I}_h w\|_{0,K}.$$

For $\|w\|_{0,K}$, $K \subset \tilde{K}$ implies that

$$(SM1.9) \quad \|w\|_{0,K} \leq \|w\|_{0,\tilde{K}} \lesssim h |\tau|_{1,\tilde{K}} = h |w|_{1,\tilde{K}},$$

where we use the Poincaré inequality with a sharp constant.

For $\|\mathcal{I}_h w\|_0$, without loss of generality, we consider the expression for $\|\mathcal{I}_h w_{11}\|$. From (SM1.5), write

$$(SM1.10) \quad (\mathcal{I}_h w_{11})|_K = \sum_{i=1}^3 a_i \phi_{z_i} + \sum_{i=1}^3 b_i \tau_{f_i} + c \varphi_K.$$

From (3.5), we have:

$$(SM1.11) \quad \begin{aligned} a_i &= \frac{1}{\#\mathcal{T}_{z_i}} \sum_{K \in \mathcal{T}_{z_i}} (Q_K w_{11})(z_i), \\ b_i &= \frac{1}{\#\mathcal{T}_{f_i}} \sum_{K \in \mathcal{T}_{f_i}} (Q_K w_{11}, 1)_{0(f_i)}, \\ c &= (w_{11}, 1)_K. \end{aligned}$$

Therefore:

$$(SM1.12) \quad \|\mathcal{I}_h w_{11}\|_{0,K} \leq \sum_{i=1}^3 |a_i| \|\phi_{z_i}\|_{0,K} + \sum_{i=1}^3 |b_i| \|\tau_{f_i}\|_{0,K} + |c| \|\varphi_K\|_{0,K} := J_1 + J_2 + J_3.$$

By the norm equivalence on a finite-dimensional space and scaling argument, we have:

$$(SM1.13) \quad \begin{aligned} |a_i| &= \frac{1}{\#\mathcal{T}_{z_i}} \left| \sum_{K \in \mathcal{T}_{z_i}} (Q_K w_{11})(z_i) \right| \leq \frac{1}{\#\mathcal{T}_{z_i}} \sum_{K \in \mathcal{T}_{z_i}} \|Q_K w_{11}\|_{L^\infty(K)} \\ &\lesssim \frac{1}{\#\mathcal{T}_{z_i}} \sum_{K \in \mathcal{T}_{z_i}} h^{-1} \|Q_K w_{11}\|_{0,K} \lesssim h^{-1} \|Q w_{11}\|_{0,\mathcal{T}(z_i)} \\ &\leq h^{-1} \|Q w_{11}\|_{0,\tilde{K}} \leq h^{-1} \|w_{11}\|_{0,\tilde{K}} \lesssim |\tau|_{1,\tilde{K}}, \end{aligned}$$

and

$$(SM1.14) \quad \|\phi_{z_i}\|_{0,K} = \|\lambda_i(3\lambda_i - 2) + \lambda_1\lambda_2\lambda_3(24 - 42\lambda_i)\|_{0,K} \lesssim h,$$

(SM1.13) and (SM1.14) mean $J_1 \lesssim h|\tau|_{1,\tilde{K}}$.

Second, by the discrete trace theorem and inverse inequality, we have:

$$(SM1.15) \quad \begin{aligned} |b_i| &= \frac{1}{\#\mathcal{T}_{f_i}} \left| \sum_{K \in \mathcal{T}_{f_i}} (Q_K w_{11}, 1)_{0(f_i)} \right| \lesssim \frac{1}{\#\mathcal{T}_{f_i}} \sum_{K \in \mathcal{T}_{f_i}} \|Q_K w_{11}\|_{0,f} \|1\|_{0,f} \\ &\lesssim \sum_{K \in \mathcal{T}_{f_i}} (h^{-\frac{1}{2}} \|Q_K w_{11}\|_{0,K} + h^{\frac{1}{2}} \|Q_K w_{11}\|_{0,K}) h^{\frac{1}{2}} \\ &= \sum_{K \in \mathcal{T}_{f_i}} (\|Q_K w_{11}\|_{0,K} + h |\tau|_{1,K}) \lesssim \sum_{K \in \mathcal{T}_{f_i}} \|Q_K w_{11}\|_{0,K} \\ &\lesssim \|Q w_{11}\|_{0,\mathcal{T}_f} \lesssim \|Q w_{11}\|_{0,\tilde{K}} \leq \|w_{11}\|_{0,\tilde{K}} \lesssim h|\tau|_{1,\tilde{K}}, \end{aligned}$$

and

$$(SM1.16) \quad \|\tau_{z_i z_j}\|_{0,K} = \left\| \frac{6}{|z_i z_j|} (\lambda_i \lambda_j + \lambda_1 \lambda_2 \lambda_3 (21\lambda_k - 12)) \right\|_{0,K} \lesssim 1.$$

(SM1.15) and (SM1.16) mean $J_2 \lesssim h|\tau|_{1,\tilde{K}}$.

Third, by the Cauchy-Schwarz inequality,

$$(SM1.17) \quad |c| \lesssim \|w_{11}\|_{0,K} \|1\|_{0,K} \lesssim h\|w_{11}\|_{0,K} \lesssim h^2|\tau|_{1,K} \leq h^2|\tau|_{1,\tilde{K}},$$

and

$$(SM1.18) \quad \|\varphi_K\|_{0,K} = \left\| \frac{1}{|K|} \lambda_1 \lambda_2 \lambda_3 (900\lambda_1 - 360\lambda_2 - 360\lambda_3) \right\|_{0,K} \lesssim h^{-1}.$$

(SM1.17) and (SM1.18) mean $J_3 \lesssim h|\tau|_{1,\tilde{K}}$. Therefore:

$$(SM1.19) \quad \|I_h w_{11}\|_{0,K} \lesssim h|\tau|_{1,\tilde{K}}.$$

Then we have:

$$(SM1.20) \quad \|\tau - \mathcal{I}_h \tau\|_0 \leq \sum_K (\|w\|_K + \|\mathcal{I}_h w\|_K) \lesssim \sum_K h|\tau|_{1,\tilde{K}} \lesssim h|\tau|_{1,\Omega}.$$

Estimating $|\mathcal{I}_h w|_1$ is nearly the same as $\|\mathcal{I}_h w\|_0$. The only differences are:

$$(SM1.21) \quad |\phi_{z_i}|_{1,K} \lesssim 1, \quad |\tau_{f_i}|_{1,K} \lesssim h^{-1}, \quad |\varphi_K|_{1,K} \lesssim h^{-2}.$$

Then we can see $|\tau - \mathcal{I}_h \tau|_1 \lesssim |\tau|_1$.

For $\|I_h \tau\|_1$, since

$$(SM1.22) \quad \|\mathcal{I}_h \tau - \tau\|_1 \lesssim \|\mathcal{I}_h \tau - \tau\|_0 + |\mathcal{I}_h \tau - \tau|_1 \lesssim |\tau|_1,$$

by Poincaré's inequality:

$$(SM1.23) \quad \|\mathcal{I}_h \tau\|_1 \leq \|\tau\|_1 + \|\mathcal{I}_h \tau - \tau\|_1 \lesssim \|\tau\|_1 + |\tau|_1 \lesssim |\tau|_1. \quad \square$$